ergic afferents [38]. In that study, m3 was more preferentially distributed in the distal dendrite region than m2, where ascending cholinergic afferent fibers tend to terminate. In both Rt neurons and interneurons, the muscarinic actions of hyperpolarization couple to increase potassium conductance [32,33]. Moreover, previous studies showed the presence of m2 in Rt by autoradiographic binding and *in situ* hybridization [30,55]. For these reasons, attention has been focused on m2 as the most important receptor in the disinhibition mechanism [5,6].

Recently, some pharmaphysiological studies of canine atrial myocytes have suggested that m3 and m4 also couple to increase potassium conductance through each channel [51,52]. Moreover, light microscopy using muscarinic-receptor-subtype-specific antibodies has shown that m2- and m3-immunolabeled neurons are present in rat and cat Rts [5,25,38,45], and that m2- and m4-immunolabeled neurons are present in mouse Rt [18].

In this study, to clarify the disinhibition mechanism of the cholinergic system, the spatial distribution pattern of three muscarinic receptor subtypes (m2–m4) in Rt was examined. Among the many sectors of Rt, the rostral part of Rt (rRt), namely, the limbic sector that reciprocally connects with limbic thalamic nuclei including AV, was focused on in this study [12–14,29,37,53]. Because both Rt and AV receive the largest number of cholinergic afferents among thalamic nuclei [26] and the neural circuit between rRt and AV has no inhibitory interneurons, this circuit is a simple model suitable for the analysis of the cholinergic system [41,58].

2. Materials and methods

2.1. Animals

Eighteen male Sprague-Dawley rats weighing 300–350 g were used in this study. Among them, seven rats were used for light microscopy experiments, six for electron microscopy experiments, and five for immunofluorescence experiments. The treatment and care of all the animals were in accordance with the European Communities Council Directive of 24 November 1986 (86/609/EEC).

2.2. Primary antibodies

In this study, three muscarinic-receptor-subtype-specific antibodies were used. The rat monoclonal antibody used for m2 had activity against a recombinant protein analogue of the third intracytoplasmic loop (i3-loop domain: amino acids 225–359) of m2 (1:1000, MAB367, clone M2-2-B3: Chemicon International Inc., Tamecula, CA, USA). It was developed by Levey et al. [27]. The rabbit polyclonal antibody used for m3 had activity against a peptide analogue of the C-terminal domain (amino acids 580–589) of m3 (1:2000, AS-3741S: Research & Diagnostic Antibodies, Berkeley, CA, USA) [3,4,36]. The mouse monoclonal antibody used for m4 was developed by Levey and Chemicon International Inc. This antibody had activity against a recombinant protein analogue of the i3-loop domain (152 amino acids) of m4 (1:5000, MAB1576, clone 17F10.2: Chemicon International Inc., Tamecula, CA, USA). For immunofluorescence experiments, a mouse monoclonal anti-parvalbumin antibody (1:4000, clone PARV-19, Sigma, St. Louis, MO, USA) was used.

2.3. Perfusion and sectioning

The rats were deeply anesthetized with an overdose of sodium pentobarbital (Nembutal 100 mg/kg body weight i.p.; Abbott Laboratories, North Chicago, IL, USA) and perfused with 100 ml of 0.2% heparinized 0.1 M phosphate buffer (PB; pH 7.4), followed by 1000 ml of a cold fixative solution in 0.1 M PB through the ascending aorta. For electron microscopy, a fixative solution containing 4% paraformaldehyde, 0.1% glutaraldehyde and 0.2% picric acid was used. For light and immunofluorescence microscopies, 3% paraformaldehyde solution was used. Following perfusion, the brains were removed and blocks of tissues containing rRt were postfixed for 3 h in the fixative described above, but without glutaraldehyde. For electron microscopy, coronal sections were prepared at a thickness of 60 μm using a vibratome and immersed in 20% sucrose in 0.1 M PB. The sections were subjected to a freeze–thaw process using liquid nitrogen to enhance the penetration of immunoreagents into the sections. The blocks of tissue used for light and immunofluorescence microscopies were immersed in 20% sucrose in 0.1 M PB overnight before sectioning in the thickness range of 50–60 μm using a freezing microtome.

2.4. Immunoperoxidase experiments for light and electron microscopies

The sections obtained for light and electron microscopies were washed three times in phosphate-buffered saline (PBS; pH 7.2) and incubated for 4 days at 4 °C on a shaker with primary antibodies against m2, m3 or m4 that were diluted at each adequate concentration with 0.1 M PBS containing 4% normal serum (normal rabbit serum for m2, normal goat serum for m3, and normal horse serum for m4). The sections were washed again in PBS, incubated overnight at 4 °C on a shaker with a secondary antibody (biotinylated rabbit anti-rat IgG for m2, biotinylated goat anti-rabbit IgG for m3, and biotinylated horse anti-mouse IgG for m4; Vector Laboratories, Burlingame, CA, USA) at a dilution of 1:200 in PBS containing 4% normal serum, washed in PBS and incubated in an avidin–biotin–peroxidase complex solution (ABC kit; Vector Laboratories, Burlingame, CA, USA) overnight at 4 °C on a shaker. They were washed again and incubated in 3,3′-diaminobenzidine (DAB: Sigma, St. Louis, MO, USA), which was diluted to 0.02% with PB containing 0.002% hydrogen peroxidase, for 5–10 min at room temperature for visualization. The sections obtained for light microscopy and some sections for electron microscopy were mounted on gelatin-coated slides, dehydrated in a graded alcohol series, cleared with xylene, and coverslipped. The sections were examined and photographed using an Olympus BX50 microscope equipped with a digital camera, DP70. The other sections for electron microscopy were treated for 1 h with PBS containing 2.5% glutaraldehyde, and postfixed for 1 h in PB containing 1% osmium tetroxide, dehydrated, and flat-embedded in Epon. Ultrathin sections were cut on an ultramicrotome using a diamond knife, collected on formvar-coated single-slot nickel grids, stained with lead citrate, and examined under a JEOL 1200 EX-II electron microscope.

Experimental controls were prepared in which the primary antibodies were omitted from the reaction solution. Light microscopy showed no immunolabeling in the control sections.

2.5. Immunofluorescence experiments

The sections obtained for immunofluorescence experiments were incubated in a mixture of two primary antibodies (anti-m2 and anti-parvalbumin antibodies, anti-m3 and anti-parvalbumin antibodies, or anti-m2 and anti-m3 antibodies) with 0.1 M PBS containing 4% normal donkey serum for 4 days at 4 °C. The sections were washed again in PBS, and incubated in a mixture of two secondary antibodies (Alexa 488 or Alexa 555 anti-rat IgG for m2 detection, Alexa 488 anti-rabbit IgG for m3 detection, and Alexa 555 anti-mouse IgG for parvalbumin detection; 1:400, Molecular Plobes, Eugene, OR, USA) with 0.1 M PBS containing 4% normal donkey serum for 3 h at room temperature.

For m4 receptor detection, single labeling was carried out using an anti-m4 antibody as the primary antibody, and Alexa 555 anti-mouse antibody as the secondary antibody.

The sections were washed three times in PBS, then briefly washed in distilled water, and mounted on slides using Gel/Mount (biomeda, Foster, CA, USA). The sections were examined and photographed using a Carl Zeiss LSM-510 confocal laser scanning microscope. The fluorescence of Alexa 488 (green) and Alexa 555 (red) dyes was analyzed using filter configurations for sequential excitation/imaging.

3. Results

3.1. Light microscopy

In light microscopy at low-power magnification of the m2-immunoreactive sections containing rRt, m2-immunolabeling was distributed throughout the rostral part of the thalamus. The immunoreactivity for m2 was high in Rt, relatively high in AV and the anterodorsal thalamic nucleus (AD), and moderate in the ventral anterior thalamic nucleus (VA) and anteromedial thalamic nucleus (AM) (Fig. 1A). At a higher magnification of Rt, very faintly m2-labeled neurons were observed to be embedded in a neuropil, in which many distinctly labeled fiberlike structures were observed (Fig. 1B). Whether these labeled structures were thin dendrite profiles or axonal fibers could not be confirmed by light microscopy.

Immunolabeling for m3 was also distributed throughout the rostral part of the thalamus. The distribution pattern of m3-immunolabeling differed from that of m2-immunolabeling (Fig. 1C). Neuronal cell bodies were distinctly labeled in the dorsomedial part of AV (AVDM), AD and VA, moderately labeled in Rt and AM, and faintly labeled in the ventrolateral part of AV (AVVL). Although the neuropil was distinctly labeled in AVVL and AD, it was relatively distinctly labeled in Rt, AVDM and VA, and moderately labeled in AM. An examination of Rt at a higher magnification revealed that m3-labeled somata and thick proximal dendrites extending from labeled somata lie within a neuropil composed of a plexus of labeled fine structures (Fig. 1D). No immunoreactivity for m4 was detected in the rostral part of the thalamus, whereas distinct immunoreactivity for m4 was observed in the striatum (Fig. 1E and F). These findings are in agreement with those of previous studies using a poly-

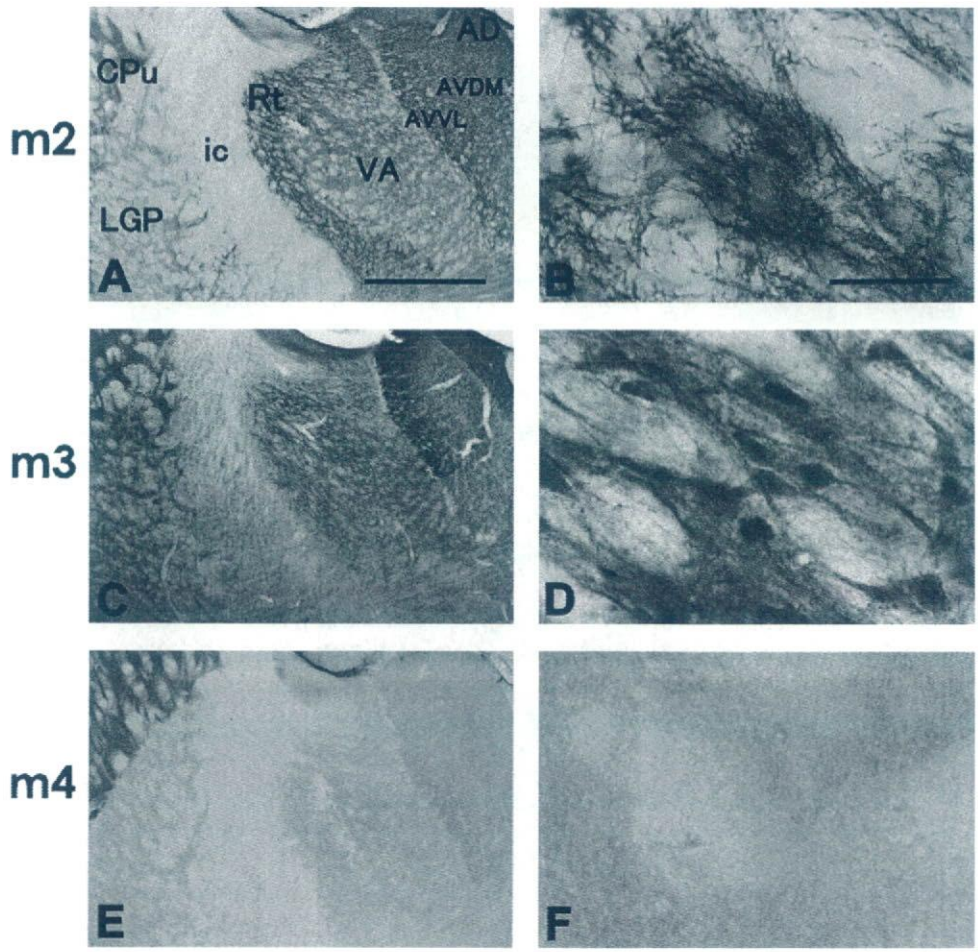

Fig. 1. Photomicrographs of m2 (A and B), m3 (C and D), and m4 (E and F) immunolabelings in rostral thalamus. Scale bars: (A, C, E) = 1 mm; (B, D, F) = 50 μm. (A) m2-immunolabeling is distributed throughout the rostral thalamic nuclei. (B) In high-magnification photomicrographs of Rt, faintly labeled neurons are embedded in a neuropil, in which many distinctly labeled fiberlike structures are observed. (C) m3-immunolabeling is also distributed throughout the rostral thalamus. (D) A high-magnification photomicrograph of Rt shows that m3-labeled somata and thick proximal dendrites extending from labeled somata lie within a neuropil composed of a plexus of labeled fine structures. (E) No immunoreactivity for m4 is detected in the rostral part of the thalamus. In CPu, however, distinct immunolabeling is observed. (F) High-magnification photomicrograph showing no m4-immunolabeling in Rt. Abbreviations: AD, anterodorsal thalamic nucleus; AVDM, dorsomedial part of anteroventral thalamic nucleus; AVVL, ventrolateral part of anteroventral thalamic nucleus; CPu, caudate putamen; ic, internal capsule; LGP, lateral globus pallidus; Rt, reticular thalamic nucleus; VA, ventral anterior thalamic nucleus.

clonal antibody against the i3-loop domain of m4 developed by Lavey et al. [17,27,57].

3.2. Immunofluorescence experiments

To clarify whether the m2- and m3-labeled profiles are rRt neuronal elements, dual-labeling experiments were carried out.

In rats, Rt consists of GABAergic inhibitory neurons [41]. These neurons also contain parvalbumin (PV) throughout their neuronal cell bodies, dendrites and axonal elements [1]. Thus, we used PV-immunoreactivity as a marker of Rt neuronal elements for dual-immunofluorescence experiments as follows. Immunoreactivity for PV distinctly labeled rRt neuronal elements (Fig. 2A and B). Immunoreactivity for m2 in immunofluorescence experiments was generally identical to that observed in the immunoperoxidase experiments (Fig. 2A). That is, numerous fiberlike structures in a neuropil were immunolabeled distinctly, whereas neuronal cell bodies were immunolabeled faintly. However, only the peripheral region of somata was labeled distinctly. Most of the PV-labeled neurons (94.9%: $N = 255$) were also m2-labeled. Furthermore, most of the fiberlike m2-labeled structures in a neuropil were also immunolabeled for PV.

Immunoreactivity for m3 in the immunofluorescence experiments was also identical to that observed in the immunoperoxidase experiments (Fig. 2B). That is, neuronal cell bodies and thick dendrites were immunolabeled distinctly. Most of the PV-labeled neurons (98.5%: $N = 482$) were also m3-labeled. These observations strongly suggest that most Rt neurons contain both m2 and m3.

Dual-labeling experiments for m2 and m3 showed that many neurons and proximal dendrites are double-labeled. In somata,

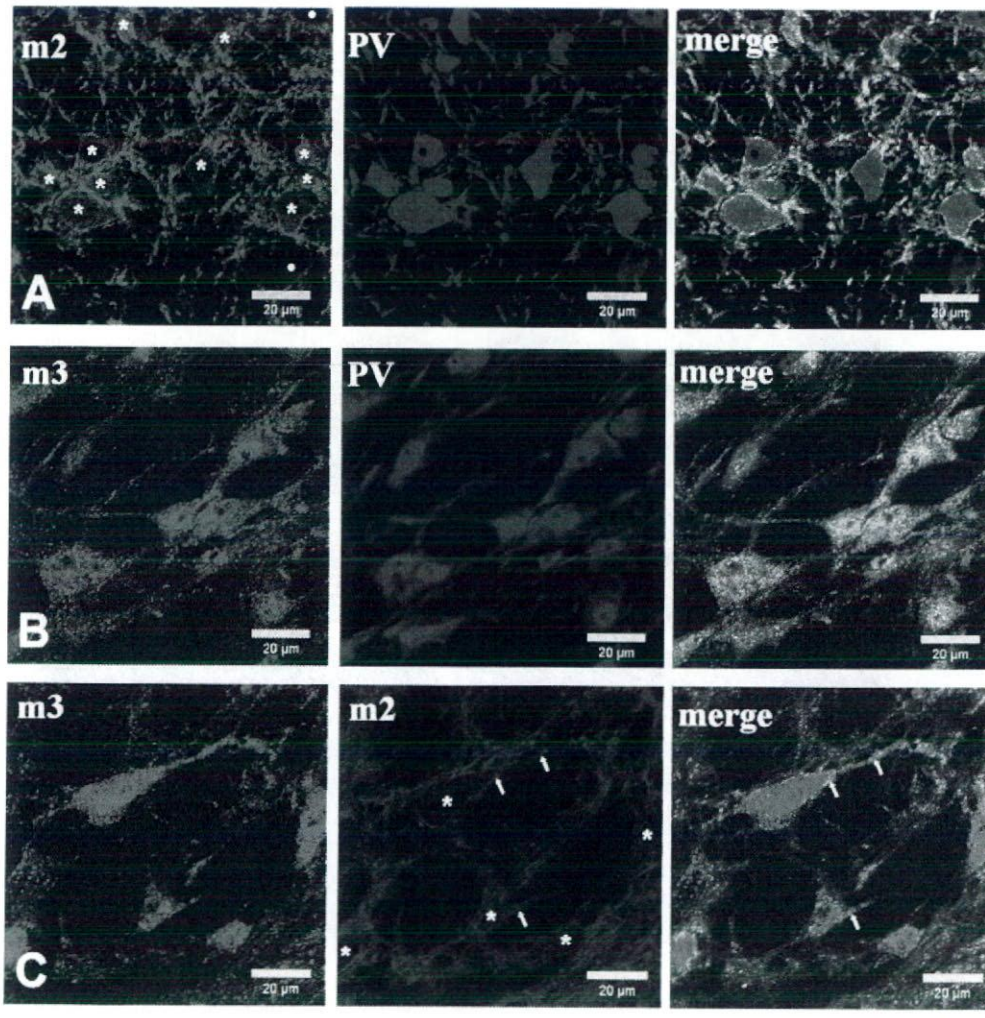

Fig. 2. Confocal microscopic images illustrating dual-immunolocalizations of m2, m3 and parvalbumin in rRt. Scale bars: 20 μm. (A) Colocalization of m2 (green) with parvalbumin (red). Distinctly m2-labeled structures are found in a neuropil and the pheripheral region of somata. Asterisks in A1 indicate dual-labeled neurons. White circles in A1 indicate m2-negative and parvalbumin-positive neurons. Most of the fine structures in the neuropil are dual-labeled. (B) Colocalization of m3 (green) with parvalbumin (red). Dual-labeling is observed in most somata and in proximal dendrites. (C) Colocalization of m3 (green) with m2 (red). Dual-labeling is observed in most somata (asterisks) and proximal dendrites (arrows). m3-labeling is distinct in somata and proximal dendrites, whereas m2-labeling is distinct in the fine structures of a neuropil and the peripheral region of somata.

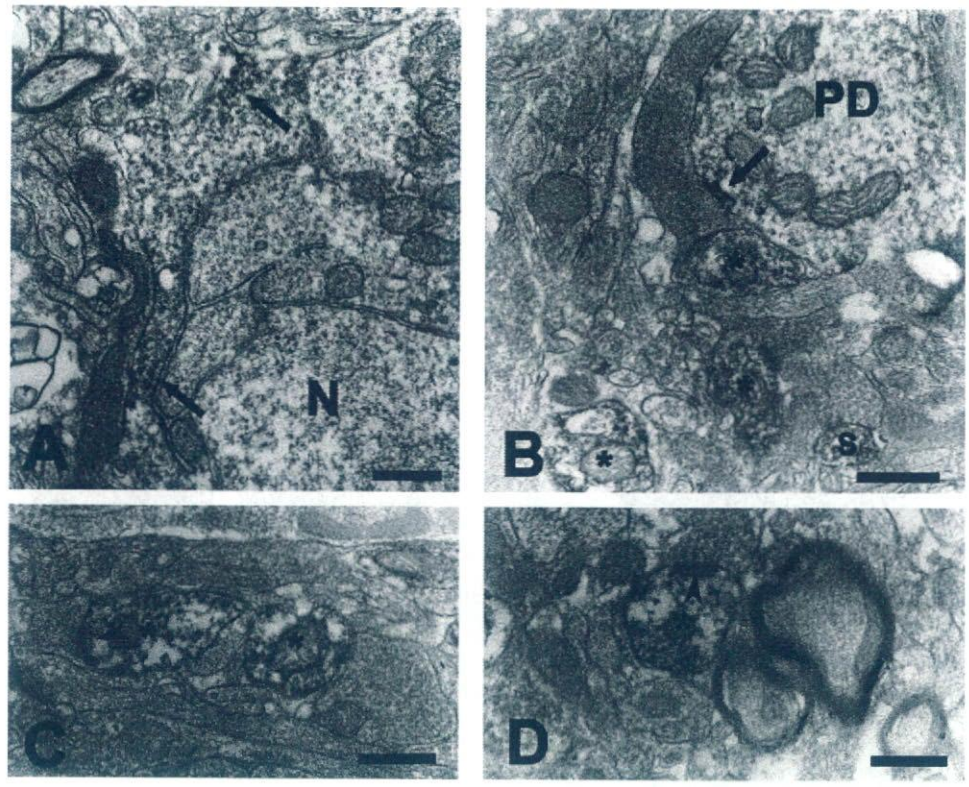

Fig. 3. Electron micrographs of m2-immunolabeling in rRt. Scale bars: 0.5 μm. (A) Low-power electron micrograph of m2-immunolabeled neuron of rRt. A few DAB reaction products (arrowheads) are distributed in the cytoplasm. They are mainly located near the cytoplasmic membrane. (B) m2-immunolabeled proximal dendrite (PD), three labeled distal dendrites (asterisks), and labeled spine (S). The immunolabeled products in PD are located near the cytoplasmic membrane (arrow). (C) Two distinctly immunolabeled distal dendrites (asterisks). One of them forms an asymmetrical synapse (arrowhead). (D) Distinctly immunolabeled distal dendrite (asterisk) forming asymmetrical synapse (arrowhead).

a large part was mainly immunolabeled for m3; however, the somata peripheral region was distinctly immunolabeled for m2. The small elements in a neuropil are predominantly immunolabeled for m2 (Fig. 2C).

No immunoreactivity for m4 was detected in the immunofluorescence experiments as well as in the immunoperoxidase experiments. Thus, no subsequent ultrastructural observation for m4 was performed.

3.3. Ultrastructural localizations of m2 and m3 receptor subtypes

To classify the m2- and m3-immunolabeled profiles in more detail, we examined the ultrastructure of immunolabeled tissues in rRt using electron microscopy.

The synaptic organization in Rt at the electron microscopy level has been well documented in previous reports [28,40,44]. In the nucleus, GABAergic neurons are predominant. In this study, we have classified dendrite profiles into three categories to analyze the distribution pattern of immunolabeling within dendrites: (1) the proximal dendrite shaft (1 μm or more in diameter, or with ribosomes), (2) the distal dendrite (0.5–1 μm in diameter, or without ribosomes) and (3) the small dendrite profile or spine (less than 0.5 μm in diameter, or without microtubules). Proximal dendrite shafts and distal dendrites generally correspond to first-order and second-order dendrites, respectively [28].

At the ultrastructural level, m2-immunolabeling indicated by the formation of DAB reaction products was observed only in neuronal somata and dendrites, and not in presynaptic terminals. The immunolabeling in cell bodies was faint, and tended to distribute in the cytoplasm near the plasma membrane (Fig. 3A). In the proximal dendrites, a small number of DAB reaction products were also found near the plasma membrane (Fig. 3B). In the distal dendrites, the immunolabeling was more distinct and additional reaction products were often associated with microtubules and the cytoplasmic membrane. Most of the immunolabeled-distal dendrite profiles were distinctly labeled throughout, thus, they were clearly identifiable from the surrounding nonlabeled structures (Fig. 3B–D).

Immunolabeling for m3 was observed only in neuronal somata and the dendrite profiles but not in the presynaptic terminals (Fig. 4). DAB reaction products in somata were widely distributed (Fig. 4A). In somata and the proximal dendrite shafts, m3-immunolabeling was more distinct than m2-immunolabeling. In a neuropil, a small number of various-sized dendrite profiles were immunolabeled for m3. In these dendrite profiles, a few DAB reaction products were found near the cytoplasmic membrane and microtubules. The immunolabeling for

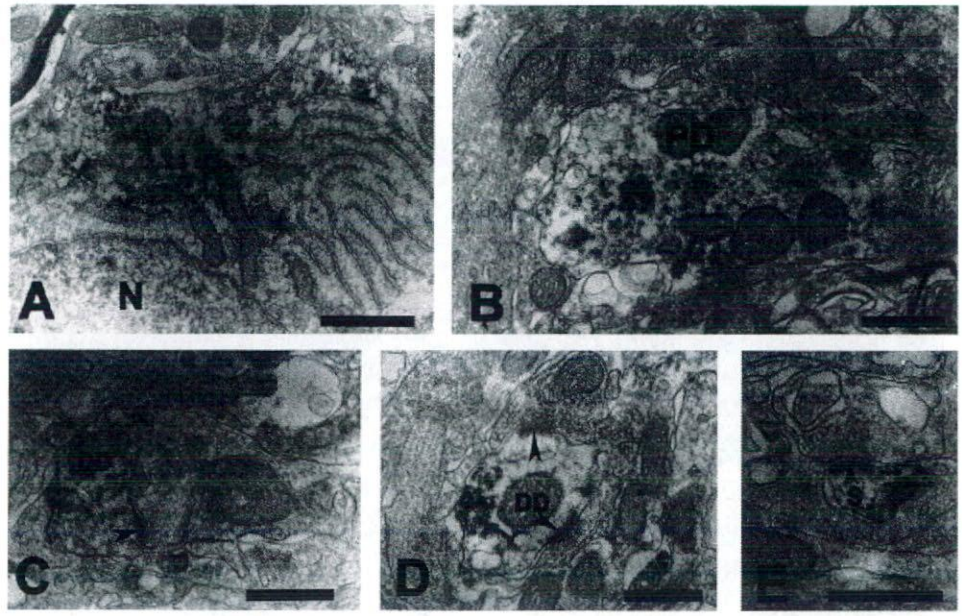

Fig. 4. Electron micrographs of m3-immunolabeling in Rt. Scale bars: (A) = 1.0 μm; (B–E) = 0.5 μm. (A) m3-immunolabeled neuron of Rt. The DAB reaction products are distributed in the cytoplasm. (B) m3-immunolabeled proximal dendrite (PD). The immunolabeled products in PD are also distributed in the cytoplasm. (C and D) Two immunolabeled distal dendrites (DD) forming asymmetrical synapses (arrowheads). (E) Immunolabeled spine (S) forming asymmetrical synapse (arrowhead).

m3 in the distal dendrite profiles was markedly less intense than that for m2.

This study demonstrated that m2-immunolabeling is preferentially distributed in distal dendrites and in the peripheral region of somata, whereas m3-immunolabeling is more preferentially distributed in somata and proximal dendrite shafts than in the distal dendrites.

4. Discussion

4.1. Localization of each receptor subtype in Rt

The immunolabeling for m2 observed using a monoclonal antibody for the i3-loop domain of m2 was most distinct in the neuropil of Rt in the rostral part of the thalamus. Additionally, the peripheral region of Rt neuronal somata was distinctly immunolabeled. These light and confocal laser scanning microscopy findings are similar to those of a previous study of cat Rt using the same antibody [5,6], and those of studies of mouse, rat and cat Rts [18,45] using a polyclonal antibody developed for the same domain of m2 [27]. This study has also shown by electron microscopy that m2-immunolabeling in Rt is preferentially distributed in the distal dendrite region and in the peripheral region of somata, and that no immunolabeling is observed in axons or fiber terminals. Previous studies of the rat and cat lateral geniculate nuclei (LGNs) have shown that, of the inhibitory elements in LGN, F2 terminals (i.e., dendrites of interneurons) are predominantly immunolabeled for m2 [5,45]. Taken together, these findings strongly suggest that the active site of m2 in the inhibitory elements of the thalamus is a dendrite rather than an axonal fiber terminal. Because cholinergic fiber terminals tend to terminate in the distal dendrite region, m2 is spatially closely associated with cholinergic afferents [16,19,20].

A polyclonal antibody for the C-terminal domain of m3 caused distinct immunolabeling in the neuropils of AVVL and AD, whereas it caused relatively distinct immunolabeling in the neuropil of Rt by light microscopy. This labeling pattern is similar to those of previous studies using a polyclonal antibody for the i3-loop domain of m3 developed by Levey et al. [25,27]. This study using confocal laser scanning and electron microscopies revealed that m3-immunolabeling is preferentially distributed in somata and the proximal dendrite region, and not in presynaptic structures.

A monoclonal antibody for the i3-loop of m4 caused no immunolabeling in the rat thalamus. This finding is in agreement with that of a previous study [45] using a polyclonal antibody for the same domain of m4 developed by Levey et al. [27]. In mice, however, their polyclonal antibody caused m4-immunolabeling in the thalamus including Rt [18]. A species difference in the distribution pattern of m4 in the thalamus may be present.

4.2. Different intracellular localizations of m2 and m3 receptor subtypes

This study revealed that most rRt neurons contain both m2 and m3 receptors with different distributions patterns. The different intracellular distribution patterns of glutamate receptors of fusiform cells in the dorsal cochlear nucleus have been reported in detail in previous studies [48–50], which showed that GluR4 and mGluR1α receptors are distributed throughout basal dendrites in which they are functional. On the other hand, in apical dendrites, in which they are not functional, these receptors are

restricted to the proximal dendrite region. These findings indicate that the intradendrite pooling site of these receptors is closely related to their functional sites. The different distribution patterns of glutamate receptors described above support the idea that m2 is more closely related to cholinergic afferents than m3 in Rt neurons.

Additionally, an *in vivo* experiment showed that the use of a muscarinic agonist, namely, oxotremorine, significantly affects the subcellular localization of m2 in striatal interneurons [2]. Thus, it is strongly suggested that the intracellular traffic system in Rt neurons transports m2 from the cell body to the distal dendrite region more actively than it transports m3. This idea is supported by the finding that m2 is often found near microtubules in distal dendrites.

However, for AV, which receives many cholinergic inputs similarly to Rt, the intracellular distribution pattern of m3 is different from that in the case of Rt. That is, in AV neurons, m3-immunolabeling is more preferentially distributed in the distal dendrite region where cholinergic afferents tend to terminate, than in somata and proximal dendrites [38,39]. Taken together, it is suggested that the active level of m3 is higher in AV neurons than in Rt neurons. A previous report also demonstrated that the distribution pattern of glutamatergic receptors for corticothalamic afferents differs between Rt and ventral posterior nuclei (VP). That is, the level of the AMPA receptor subunit GluR4 is higher in Rt than in VP [35]. It seems likely that a comparison of the distribution pattern of each receptor between Rt and thalamic nuclei is useful for understanding intrathalamic neural circuits.

A question still remains: What is the role of m3 in Rt neurons? Because the colocalization of different types of metabolic receptor in a neuron is generally observed, the possibility that m3 acts at an undetectably low level, as determined by electrophysiological studies, cannot be excluded.

4.3. Functional implications of receptor subtypes in rRt-AV circuit

rRt is reciprocally connected with limbic thalamic nuclei including AV. In the rat, the neural circuit between rRt and AV is devoid of inhibitory interneurons; thus, it is considered to be a simpler model circuit than other reticulothalamic connections such as visual systems [41,58]. A hypothetical schematic diagram is shown in Fig. 5. In the circuit between rRt and AV, rRt neurons receive glutamatergic excitatory inputs from AV neurons as collaterals of thalamocortical projections, and conversely send GABAergic inhibitory outputs to AV neurons [13,14,29,37,53]. Both nuclei receive the highest number of cholinergic afferents among the thalamic nuclei [26].

In this study, we revealed that m2 immunolocalization is more closely associated with cholinergic afferents than m3 immunolocalization in rRt. On the other hand, a previous study showed that m3 is more closely associated with cholinergic afferents than m2 in AV [38]. These morphological findings strongly support the findings of electrophysiological studies suggesting that cholinergic afferents play an important role in the facilitation of the thalamocortical pathway. First, the electrical stimulation of the laterodorsal tegmental nucleus induces long-lasting enhancement of the responsiveness of AV neurons to mammillary body stimuli. This enhancement is blocked by the application of scopolamine, a muscarinic antagonist [42]. Because m3 decreases M-current, it may block the adaptation of AV neurons. Thus, it seems likely that the increase in AV neuronal activity is dependent on m3. Second, the electric stimulation of the cat brainstem inhibits the GABAergic neuronal activity of the perigeniculate nucleus (PGN), the cat visual sector of Rt, with a long-lasting hyperpolarization of membrane potential via potassium conductance [21]. Recent reports suggested that both m2 and m3 increase potassium conductance [51,52]. This study suggests that m2 is predominant in distal dendrites where cholinergic afferents tend to terminate. In short, it seems likely that cholinergic systems directly excite AV relay neurons through m3, and indirectly facilitate thalamocortical transmission by disinhibition through m2 of Rt neurons.

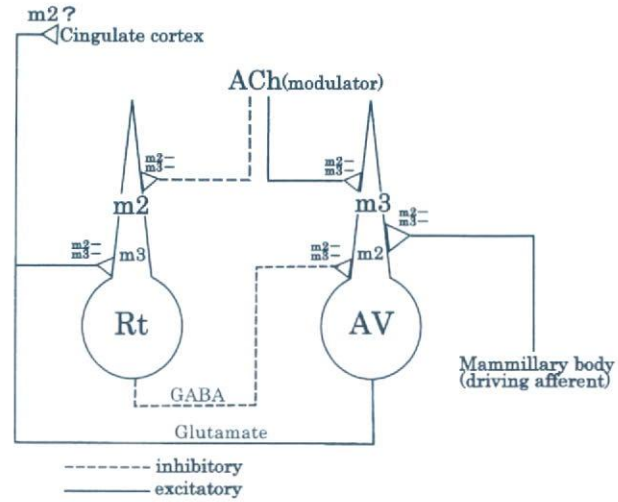

Fig. 5. Hypothetical schematic diagram illustrating neuronal circuit between Rt and AV. Cholinergic efferents preferentially terminate in the distal region of the dendrites of both neurons. In this region, m2 is predominant in Rt neurons, whereas m3 is predominant in AV neurons. In the hypothesis of this study, cholinergic systems directly excite AV relay neurons through m3, and indirectly disinhibit AV relay neurons through m2 of Rt neurons. In rRt and AV, neither m2 nor m3 was detected in axonal elements (present study) [38]; however, previous autoradiography experiments suggested that thalamocortical terminals derived from AV contain m2 [10,56].

Cholinergic afferents of AV are exclusively derived from the brainstem cholinergic center; however, Rt receives additional afferents from another cholinergic center, namely, the basal forebrain [9,15,23]. Because the stimulation of the basal forebrain also causes the transition of the Rt neuronal firing mode to the burst firing mode [43], it seems likely that both cholinergic centers participate in the disinhibition mechanism. A previous study showed that cholinergic terminals derived from the basal forebrain contain $p75^{NTR}$ [8]. Cholinergic afferents from the basal forebrain may play an important role in the development of the neural circuit.

In this study, we propose a hypothetical model of a cholinergic system using a simple neuronal circuit between rRt and AV that lacks inhibitory interneurons.

Conflict of interest

No conflict of interest exists in relation to the authors in this manuscript and the content.

Acknowledgement

This work was supported by a project research grant (No. 17-10) from Toho University School of Medicine.

References

[1] A. Amadeo, B. Ortino, C. Frassoni, Parvalbumin and GABA in the developing somatosensory thalamus of the rat: an immunocytochemical ultrastructural correlation, Anat. Embryol. 203 (2001) 109–119.
[2] V. Bernard, O. Laribi, A.I. Levey, B. Bloch, Subcellular redistribution of m2 muscarinic acetylcholine receptors in striatal interneurons *in vivo* after acute cholinergic stimulation, J. Neurosci. 18 (1998) 10207–10218.
[3] R. Buchli, A. Ndoye, J. Arredondo, R.J. Webber, S.A. Grando, Identification and characterization of muscarinic acetylcholine receptor subtypes expressed in human skin melanocytes, Mol. Cell. Biochem. 228 (2001) 57–72.
[4] R. Buchli, A. Ndoye, J.G. Rodriguez, S. Zia, R.J. Webber, S.A. Grando, Human skin fibroblast express m2, m4, and m5 subtypes of muscarinic acetylcholine receptors, J. Cell. Biochem. 74 (1999) 264–277.
[5] W.B. Carden, M.E. Bickford, Location of muscarinic type 2 receptors within the synaptic circuitry of the cat visual thalamus, J. Comp. Neurol. 410 (1999) 431–443.
[6] W.B. Carden, M.E. Bickford, The location of muscarinic type 2 receptors within the synaptic circuitry of the cat lateral posterior nucleus, Neurosci. Lett. 276 (1999) 153–156.
[7] M.P. Caulfield, Muscarinic receptors—characterization, coupling and function, Pharmac. Ther. 58 (1993) 319–379.
[8] S. Chen, M. Bentivoglio, Nerve growth factor receptor-containing cholinergic neurons of the basal forebrain project to the thalamic reticular nucleus in the rat, Brain Res. 606 (1993) 207–212.
[9] J. Cornwall, J.D. Cooper, O.T. Phillipson, Projections to the rostral reticular thalamic nucleus in the rat, Exp. Brain Res. 80 (1990) 157–171.
[10] K.L. Dopke, K.E. Vrana, L.J. Vogt, B.A. Vogt, AF-DX 384 binding in rabbit cingulate cortex: two site kinetics and section autoradiography, J. Pharmacol. Exp. Ther. 274 (1995) 562–569.
[11] R.C. Dossi, D. Paré, M. Steriade, Short-lasting nicotinic and long-lasting muscarinic depolarizing responses of thalamocortical neurons to stimulation of mesopontine cholinergic nuclei, J. Neurophysiol. 65 (1991) 393–406.
[12] A. Gonzalo-Ruiz, A.R. Lieberman, Topographic organization of projections from the thalamic reticular nucleus to the anterior thalamic nuclei in the rat, Brain Res. Bull. 37 (1995) 17–35.
[13] A. Gonzalo-Ruiz, A.R. Lieberman, GABAergic projections from the thalamic reticular nucleus to the anteroventral and anterodorsal thalamic nuclei of the rat, J. Chem. Neuroanat. 9 (1995) 165–174.
[14] A. Gonzalo-Ruiz, L. Morte, A.R. Lieberman, Evidence for collateral projections to the retrosplenial granular cortex and thalamic reticular nucleus from glutamate and/or aspartate-containing neurons of the anterior thalamic nuclei in the rat, Exp. Brain Res. 116 (1997) 63–72.
[15] A.E. Hallanger, A.I. Levey, H.J. Lee, D.B. Rye, B.H. Wainer, The origins of cholinergic and other subcortical afferents to the thalamus in the rat, J. Comp. Neurol. 262 (1987) 105–124.
[16] A.E. Hallanger, B.H. Wainer, Ultrastructue of ChAT-immunoreactive synaptic terminals in the thalamic reticular nucleus of the rat, J. Comp. Neurol. 278 (1988) 486–497.
[17] S.M. Hersch, A.I. Levey, Diverse pre- and post-synaptic expression of m1–m4 muscarinic receptor proteins in neurons and afferents in the rat neostriatum, Life Sci. 56 (1995) 931–938.
[18] C.F. Hohmann, E.D. Potter, A.I. Levey, Development of muscarinic receptor subtypes in the forebrain of the mouse, J. Comp. Neurol. 358 (1995) 88–101.
[19] C.R. Houser, P.E. Phelps, J.E. Vaughn, Cholinergic innervation of the rat thalamus as demonstrated by the immunocytochemical localization of choline acetyltransferase, in: M. Bentivoglio, R. Spreafico (Eds.), Cellular Thalamic Mechanisms, Elsevier, Amsterdam, 1988, pp. 387–398.
[20] C.R. Houser, Cholinergic synapses in the central nervous system: studies of the immunocytochemical localization of choline acetyltransferase, J. Electron Microsc. Tech. 15 (1990) 2–19.
[21] B. Hu, M. Steriade, M. Deschênes, The effects of brainstem peribrachial stimulation on perigeniculate neurons: the blockage of spindle waves, Neuroscience 31 (1989) 1–12.
[22] E.C. Hulme, N.J.M. Birdsall, N.J. Buckley, Muscarinic receptor subtypes, Annu. Rev. Pharmacol. Toxicol. 30 (1990) 633–673.
[23] A. Jourdain, K. Semba, H.C. Fibiger, Basal forebrain and mesopontine tegmental projections to the reticular thalamic nucleus: an axonal collateralization and immunohistochemical study in the rat, Brain Res. 505 (1989) 55–65.
[24] K.H. Lee, D.A. McCormick, Acetylcholine excites GABAergic neurons of the ferret perigeniculate nucleus through nicotinic receptors, J. Neurophysiol. 73 (1995) 2123–2128.
[25] A.I. Levey, S.M. Edmunds, C.J. Heilman, T.J. Desmond, K.A. Frey, Localization of muscarinic m3 receptor protein and M3 receptor binding in rat brain, Neuroscience 63 (1994) 207–221.
[26] A.I. Levey, A.E. Hallanger, B.H. Wainer, Choline acetyltransferase immunoreactivity in the rat thalamus, J. Comp. Neurol. 257 (1987) 317–332.
[27] A.I. Levey, C.A. Kitt, W.F. Simonds, D.L. Price, M.R. Brann, Identification and localization of muscarinic acetylcholine receptor proteins in brain with subtype-specific antibodies, J. Neurosci. 11 (1991) 3218–3226.
[28] X.-B. Liu, E.G. Jones, Predominance of corticothalamic synaptic inputs to thalamic reticular nucleus neurons in the rat, J. Comp. Neurol. 414 (1999) 67–79.
[29] D.A. Lozsádi, Organization of connections between the thalamic reticular and the anterior thalamic nuclei in the rat, J. Comp. Neurol. 358 (1995) 233–246.
[30] D.C. Mash, L.T. Potter, Autoradiographic localization of M1 and M2 muscarine receptors in the rat brain, Neuroscience 19 (1986) 551–564.
[31] D.A. McCormick, Cellular mechanisms underlying cholinergic and noradrenergic modulation of neuronal firing mode in the cat and guinea pig dorsal lateral geniculate nucleus, J. Neurosci. 12 (1992) 278–289.
[32] D.A. McCormick, H.-C. Pape, Acetylcholine inhibits identified interneurons in the cat lateral geniculate nucleus, Nature 334 (1988) 246–248.
[33] D.A. McCormick, D.A. Prince, Acetylcholine induces burst firing in thalamic reticular neurones by activating a potassium conductance, Nature 319 (1986) 402–405.
[34] D.A. McCormick, Neurotransmitter actions in the thalamus and cerebral cortex and their role in neuromodulation of thalamocortical activity, Prog. Neurobiol. 39 (1992) 337–388.
[35] E.M. Mineff, R.J. Weinberg, Differential synaptic distribution of AMPA receptor subunits in the ventral posterior and reticular thalamic nuclei of the rat, Neuroscience 101 (2000) 969–982.
[36] A. Ndoye, R. Buchli, B. Greenberg, V.T. Nguyen, S. Zia, J.G. Rodriguez, R.J. Webber, M.A. Lawry, S.A. Grando, Identification and mapping of keratinocyte muscarinic acetylcholine receptor subtypes in human epidermis, J. Invest. Dermatol. 111 (1998) 410–416.
[37] S. Oda, M. Kuroda, S.Y. Chen, M. Shinkai, K. Kishi, Ultrastructure and distribution of axon terminals from the reticular thalamic nucleus to the anteroventral thalamic nucleus of the rat, J. Brain Res. 37 (1996) 459–466.
[38] S. Oda, M. Kuroda, S. Kakuta, K. Kishi, Differential immunolocalization of m2 and m3 muscarinic receptors in the anteroventral and anterodorsal thalamic nuclei of the rat, Brain Res. 894 (2001) 109–120.
[39] S. Oda, M. Kuroda, S. Kakuta, S. Tanihata, Y. Ishikawa, K. Kishi, Ultrastructure of ascending cholinergic terminals in the anteroventral thalamic nucleus of the rat: a comparison with the mammillothalamic terminals, Brain Res. Bull. 59 (2003) 473–483.

[40] P.T. Ohara, A.R. Lieberman, The thalamic reticular nucleus of the adult rat: experimental anatomical studies, J. Neurocytol. 14 (1985) 365–411.
[41] O.P. Ottersen, J. Storm-Mathisen, GABA-containing neurons in the thalamus and pretectum of the rodent, Anat. Embryol. 170 (1984) 197–207.
[42] D. Paré, M. Steriade, M. Deschênes, D. Bouhassira, Prolonged enhancement of anterior thalamic synaptic responsiveness by stimulation of a brain-stem cholinergic group, J. Neurosci. 10 (1990) 20–33.
[43] D. Pinault, M. Deschênes, Muscarinic inhibition of reticular thalamic cells by basal forebrain neurons, Neuroreport 3 (1992) 1101–1104.
[44] D. Pinault, Y. Smith, M. Deschênes, Dendrodendritic and axoaxonic synapses in the thalamic reticular nucleus of the adult rat, J. Neurosci. 17 (1997) 3215–3233.
[45] K.L. Plummer, K.A. Manning, A.I. Levey, H.D. Rees, D.J. Uhlrich, Muscarinic receptor subtypes in the lateral geniculate nucleus: a light and electron microscopic analysis, J. Comp. Neurol. 404 (1999) 408–425.
[46] K. Racké, U.R. Juergens, S. Matthiesen, Control by cholinergic mechanisms, Eur. J. Pharmacol. 533 (2006) 57–68.
[47] P.P. Rowell, K.A. Volk, J. Li, M.E. Bickford, Investigations of the cholinergic modulation of GABA release in rat thalamus slices, Neuroscience 116 (2003) 447–453.
[48] M.E. Rubio, R.J. Wenthold, Glutamate receptors are selectively targeted to postsynaptic sites in neurons, Neuron 18 (1997) 939–950.
[49] M.E. Rubio, R.J. Wenthold, Differential distribution of intracellular glutamate receptors in dendrites, J. Neurosci. 19 (1999) 5549–5562.
[50] M.E. Rubio, Selective targeting of glutamate receptors in neurons, Mol. Neurobiol. 21 (2000) 1–19.
[51] H. Shi, H. Wang, Z. Wang, Identification and characterization of multiple subtypes of muscarinic acetylcholine receptors and their physiological functions in canine hearts, Mol. Pharmacol. 55 (1999) 497–507.
[52] H. Shi, B. Yang, D. Xu, H. Wang, Z. Wang, Electrophysiological characterization of cardiac muscarinic acetylcholine receptors: different subtypes mediate different potassium currents, Cell. Physiol. Biochem. 13 (2003) 59–74.
[53] H. Shibata, Topographic organization of subcortical projections to the anterior thalamic nuclei in the rat, J. Comp. Neurol. 323 (1992) 117–127.
[54] M. Steriade, Acetylcholine systems and rhythmic activities during the waking–sleep cycle, Prog. Brain Res. 145 (2004) 179–196.
[55] M.T. Vilaró, K.-H. Wiederhold, J.M. Palacios, G. Mengod, Muscarinic M_2 receptor mRNA expression and receptor binding in cholinergic and non-cholinergic cells in the rat brain: a correlative study using *in situ* hybridization histochemistry and receptor autoradiography, Neuroscience 47 (1992) 367–393.
[56] B.A. Vogt, P.B. Crino, E.L. Jensen, Multiple heteroreceptors on limbic thalamic axons: M_2 acetylcholine, serotonin$_{1B}$, β_2-adrenoceptors, μ-opioid, and neurotensin, Synapse 10 (1992) 44–53.
[57] L.A. Volpicelli, A.I. Levey, Muscarinic acetylcholine receptor subtypes in cerebral cortex and hippocampus, Prog. Brain Res. 145 (2004) 59–65.
[58] B. Wang, A. Gonzalo-Ruiz, J.M. Sanz, G. Campbell, A.R. Lieberman, Immunoelectron microscopic study of γ-aminobutyric acid inputs to identified thalamocortical projection neurons in the anterior thalamus of the rat, Exp. Brain Res. 126 (1999) 369–382.
[59] J.J. Zhu, D.J. Uhlrich, Cellular mechanisms underlying two muscarinic receptor-mediated depolarizing responses in relay cells of the rat lateral geniculate nucleus, Neuroscience 87 (1998) 767–781.

研究成果の刊行物・別刷

平成１７年度～平成１８年度

Available online at www.sciencedirect.com
ScienceDirect
Bioorganic & Medicinal Chemistry 14 (2006) 8014–8031
Bioorganic & Medicinal Chemistry

Design, synthesis, and BK channel-opening activity of hexahydrodibenzazepinone derivatives

Toshihiko Tashima,[a] Yoshimi Toriumi,[a] Yumi Mochizuki,[a] Taro Nonomura,[a] Satoru Nagaoka,[a] Katsuo Furukawa,[b] Hiromichi Tsuru,[b] Satomi Adachi-Akahane[b] and Tomohiko Ohwada[a,*]

[a]*Graduate School of Pharmaceutical Sciences, The University of Tokyo, Laboratory of Organic and Medicinal Chemistry, 7-3-1 Hongo, Bunkyo-ku, Tokyo 113-0033, Japan*
[b]*Department of Pharmacology, Faculty of Medicine, School of Medicine, Toho University, 5-21-16, Omori-Nishi, Ota-ku, Tokyo 143-8540, Japan*

Received 19 June 2006; revised 21 July 2006; accepted 22 July 2006
Available online 10 August 2006

Abstract—In order to explore new scaffolds for large-conductance Ca^{2+}-activated K^+ channel (BK channel) openers, we carried out molecular design and synthesis on the basis of the following two concepts: (1) introduction of a heteroatom into the dehydroabietic acid (BK channel opener) skeleton would allow easier introduction of substituents. (2) Because of the fourfold symmetrical structure of BK channels, dimeric compounds in which two pharmacophores are linked through a tether are expected to have a greater binding probability to the channels, resulting in increased channel-opening activity. Herein, we explore the usefulness of the hexahydrodibenzazepinone structure as a new scaffold for BK channel openers. The synthesized monomer compounds of hexahydrodibenzazepinone derivatives, which can be derived from dehydroabietic acid, were subjected to electrophysiological patch–clamp studies, followed by Magnus contraction–relaxation assay using rabbit urinary bladder smooth muscle strips to assess overall activities. Dimeric compounds were designed by linking the monomeric hexahydrodibenzazepinone derivatives through a diacetylenebenzene tether, and their channel-opening activities were evaluated by electrophysiological methods. Finally, we concluded that the critical structure for BK channel-opening activity is the hexahydrodibenzazepinone monomer substituted with a phenyl-bearing alkynyl substituent on the lactam amide.

1. Introduction

Ion-selective channels are membrane proteins, which generate electrical ionic signals and regulate signal transduction events in living systems. Among such channels, K^+ channels are widely expressed in various tissues, such as smooth muscles and neurons, and play an important role in modulating membrane potential. In particular, large-conductance Ca^{2+}-activated K^+ channels (BK channels) elicit such a large K^+ conductance that depolarized membrane potential can be effectively quenched by the opening of BK channels.[1] The BK channels are distributed in both excitable and non-excitable cells, which are involved in many cellular functions,[2] such as action potential repolarization, neuronal excitability, neurotransmitter release, hormone secretion, tuning of cochlear hair cells,[3] innate immunity,[4] and modulation of the tone of vascular, airway, uterine, gastrointestinal, and urinary bladder smooth muscle tissues. Since BK channels are activated by both elevation of intracellular Ca^{2+} concentration and membrane depolarization, the K^+ efflux via BK channels results in membrane repolarization and the suppression of Ca^{2+} influx through voltage-dependent Ca^{2+} channels. Accordingly, BK channels serve as a negative-feedback mechanism to relax excessive muscle contraction in smooth muscles[5] and to prevent aberrant cellular excitability of neurons.

Like other members of the voltage-dependent K^+ channel superfamily, BK channels are tetrameric proteins composed of pore-forming α-subunits and auxiliary β-subunits.[6] Thus, the K^+ channels are fourfold symmetrical. Each BK channel α-subunit contains seven transmembrane spanning segments S0–S6 at the N-terminus

Keywords: BK channel opener; Hexahydrodibenzazepinones; Dimeric compound; K^+ channel.
* Corresponding author. Tel.: +81 3 5841 4730; fax: +81 3 5841 4735; e-mail: ohwada@mol.f.u-tokyo.ac.jp

0968-0896/$ - see front matter © 2006 Elsevier Ltd. All rights reserved.
doi:10.1016/j.bmc.2006.07.042

and the four hydrophobic segments S7–S10 at the large intracellular C-terminus. Unlike other classes of Ca^{2+}-activated K^+ channels, SK (small-conductance) and IK (intermediate conductance) channels, the α-subunit of the BK channels has an extra hydrophobic transmembrane segment (S0) that leads to the extracellular N-terminus. The N-terminus acts as a binding domain for β-subunits.[7] Each α-subunit has a S4 voltage sensor[8] and a pore-forming region formed by S5–S6 and the P-loop.

BK channel openers have potential therapeutic applications because of possible involvement of BK channels in various pathophysiological conditions such as hypertension,[9] coronary artery spasm, urinary incontinence,[10] progressive deafness,[11] and several neurological disorders.[12] The BK channel has an advantage as a therapeutic target compared to other K^+ channels, such as the ATP-sensitive potassium channel (K_{ATP}), because it is mostly absent in cardiac myocytes, except for mitochondria.[13] The BK channel openers comprise a large series of synthetic benzimidazolone derivatives (Chart 1), such as NS004[14] and NS1619,[15] the biaryl amines, such as mefenamic and flufenamic acids,[16] the biarylureas, such as NS1608,[17] the aryloxindoles (BMS-204352),[18] the arylpyrroles (NS-8),[19] indole-3-carboxylic acid esters (CGS-7184, CGS-7181)[20] and natural modulators, including dihydrosoyasaponin-1 (dehydrosoyasaponin-1, DHS-1),[21] and terpenes such as maxikdiol (**1**, Chart 2).[22] Most of these compounds activate BK channels as a subsidiary action in addition to their primary action.[23] In this context, the available scaffolds for BK channel openers are rather limited in structural diversity. Both of the pioneering drugs NS004 and NS1619 are α-subunit-selective BK openers. We have found that

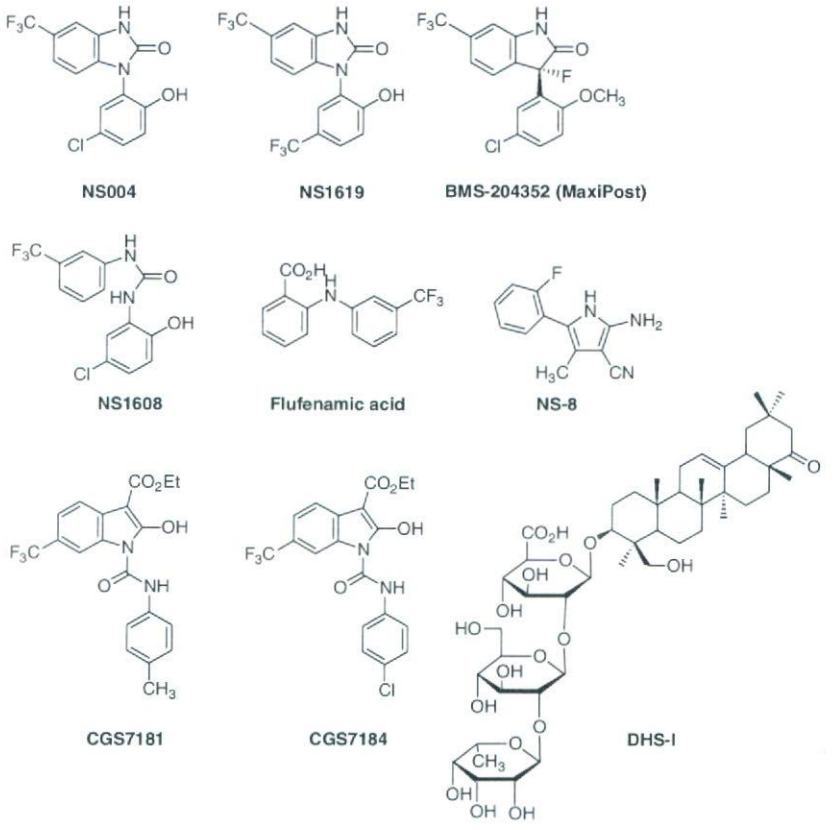

Chart 1.

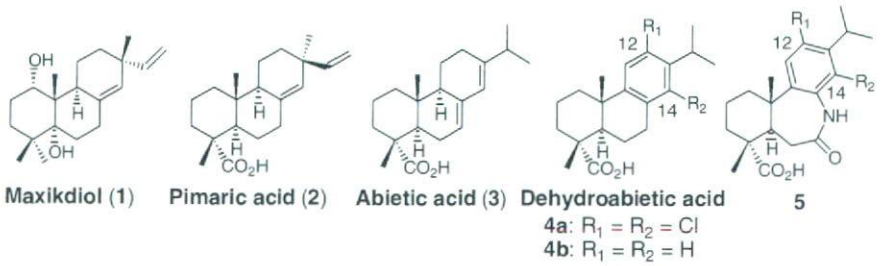

Chart 2.

pimaric acid and dehydroabietic acid act as BK channel openers via direct interaction with the α-subunit of BK channels.[24] Several possible mechanisms can explain the effect of the activators on BK channels: (i) modulation of the gating (=open/close) kinetics of the α subunit, (ii) modulation of the Ca^{2+} binding site at the C-terminal end of the α-subunit, (iii) strengthening of the interaction between the α- and β-subunits, and (iv) mimicking the interaction of β- with the α-binding site. Novel synthetic channel modulators would be useful tools to reveal the mechanism of the channel gating at the atomic level, in addition to having therapeutic potential.

We have already found that pimaric acid (**2**) and dehydroabietic acid (**4**) exhibit BK channel opening activities, while the structurally related abietic acid (**3**) has weak activity (Chart 2).[24] In order to explore new structural scaffolds for BK channel openers, we carried out molecular design on the basis of two concepts: (1) introduction of a heteroatom into the dehydroabietic acid skeleton would allow easier introduction of substituents. (2) Because of the fourfold symmetrical structure of the BK channels, dimeric compounds in which two pharmacophores are linked through a tether may have a greater binding probability to the channels, resulting in increased channel opening activity. Herein we describe our exploration of the hexahydrodibenzazepinone derivatives (**5**), which can be generated from dehydroabietic acid (**4**), to examine the value of the hexahydrodibenzazepinone structure as a new scaffold for BK channel openers.

The synthesized monomer compounds were evaluated by means of electrophysiological patch–clamp studies in HEK293 cells expressing BK channels, followed by the Magnus contraction–relaxation assay with rabbit urinary bladder smooth muscle strips to evaluate overall actions on smooth muscle. Dimeric compounds were designed on the basis of the monomeric scaffolds, and their channel opening activities were evaluated by electrophysiological methods. Our results demonstrate that the hexahydrodibenzazepinone structure is a potential new scaffold for novel BK channel openers.

2. Chemistry

2.1. Hexahydrodibenzazepinone derivatives

The hexahydrodibenzazepinone derivatives (**11a** and **b**) were synthesized as shown in Scheme 1. The benzylic oxidation of the dehydroabietic acid derivatives (**6a** and **b**) was carried out with CrO_3 in Ac_2O/AcOH to give the corresponding ketone compounds (**7a** and **b**). The ketones were converted to the oximes (**8a** and **b**), and the hydroxyl group of the oximes was tosylated. These tosylated oximes (**9a** and **b**) were subjected to the Beck-

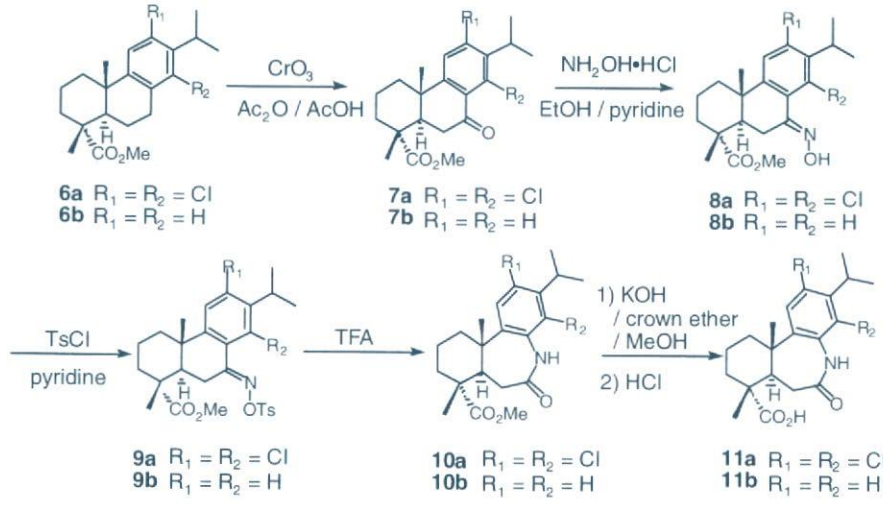

Scheme 1.

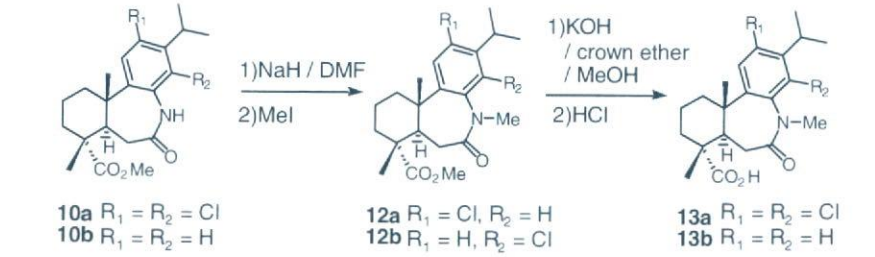

Scheme 2.

mann rearrangement in the presence of TFA at rt to give the hexahydrodibenzazepinone derivatives (**10a** and **b**). Finally, the methyl ester was hydrolyzed with KOH and crown ether in methanol to give the corresponding carboxylic acids (**11a** and **b**). The *N*-methyl group was introduced with methyl iodide after deprotonation of

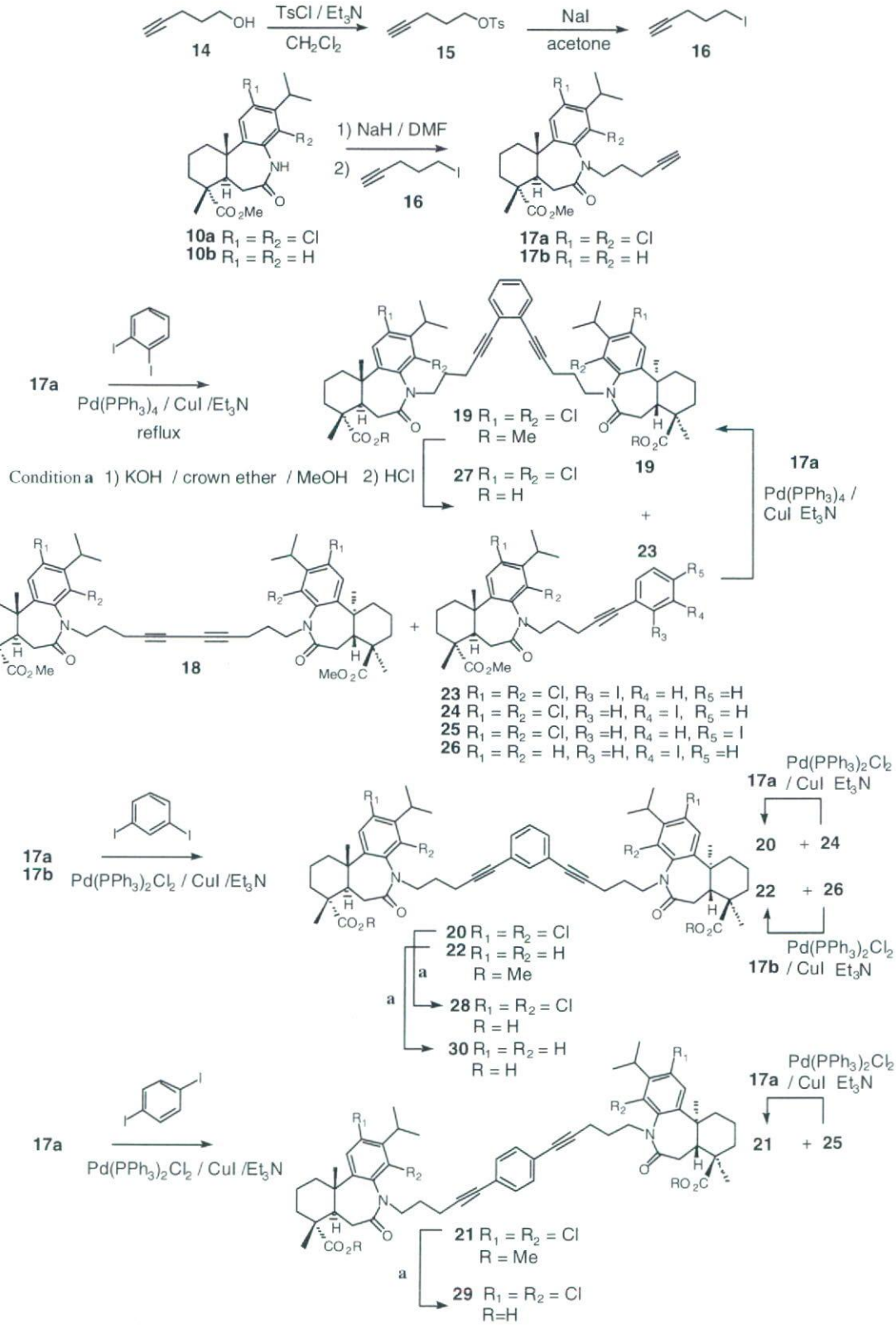

Scheme 3.

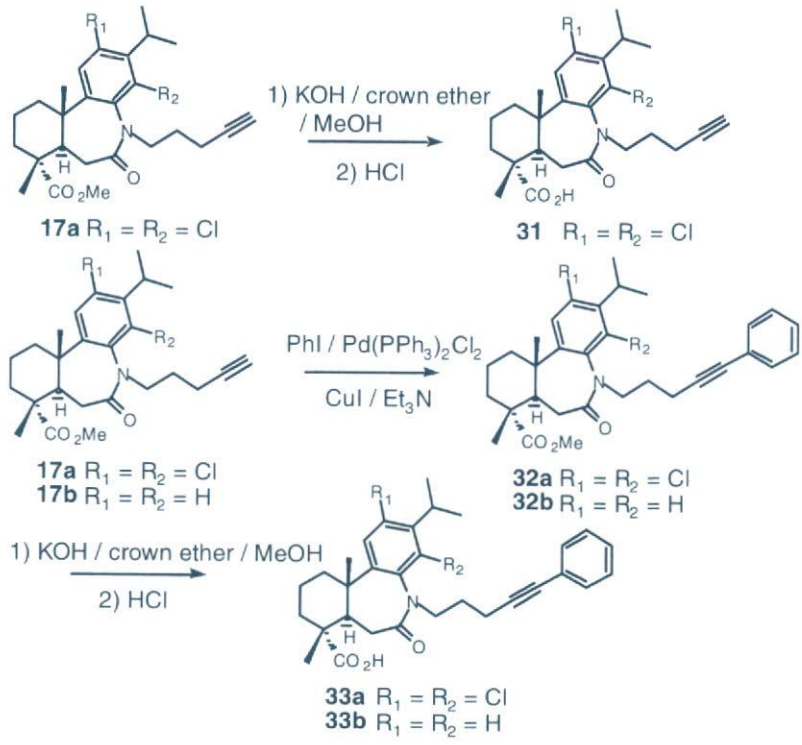

Scheme 4.

the amide NH group with NaH (Scheme 2). Hydrolysis of the methyl ester was carried out in a similar manner to that described for **10**, to give the carboxylic acids (**13a** and **b**). The lactam structure of hexahydrodibenzazepinone derived from the Beckmann rearrangement was reported previously,[25] and our ^{1}H NOE analysis between the N–CH_3 group and the aromatic protons of the compound **12a** confirmed the structure.

The syntheses of the dimeric compounds (**27–30**) are illustrated in Scheme 3. Sonogashira coupling was the key reaction. With respect to the linker moiety, 4-pentyn-1-ol (**14**) was tosylated and converted to the iodide (**16**) with NaI. N-Alkylation was carried out with the iodide **16** to afford the alkyne derivatives (**17a,b**), which were coupled with *m*-diiodobenzene or *p*-diiodobenzene in the presence of $Pd(PPh_3)_2Cl_2$/CuI in Et_3N at rt (the Sonogashira coupling reaction). The acetylene disubstituted products (**20–22**) and/or the acetylene monosubstituted products (**24–26**) were obtained. In the case of the monosubstituted products, a second Sonogashira coupling reaction was carried out to obtain the acetylene disubstituted products (**20–22**). Finally, the ester group was hydrolyzed with KOH and crown ether in methanol to afford the corresponding dimeric compounds (**27–29**). The alkyne (**17**) and *o*-diiodobenzene did not readily undergo the Sonogashira coupling reaction with $Pd(PPh_3)_2Cl_2$/CuI in Et_3N at rt. Under these reaction conditions, in addition to the acetylene monosubstituted product (**23**), the acetylene homodimeric product (**18**) was obtained, probably because of steric hindrance. Thus, on coupling of the alkyne (**17a**) with *o*-diiodobenzene, $Pd(PPh_3)_4$ was used as a catalyst and purified CuI was used under reflux in Et_3N, to give the desired ortho dimeric compound (**19**). Hydrolysis of the ester provided the final carboxylic acid (**27**). The monomeric compounds (**31** and **33a,b**), which bear a alkynyl substituent on the lactam amide, were also synthesized as shown in Scheme 4.

2.2. Molecular design of dimers

The X-ray structures of several K^+ channels revealed that the diameters of the pores (the gate region) in the closed state are 6 Å (for the KcsA channel) and 8 Å (KirBac channel), and those in open state are 25 Å (for the MthK channel) and 19 Å (KvAP channel). In the cases of other ion channels, the binding sites of small organic molecules, such as channel blockers, are located on the inner side of the pore.[26] Moreover, the dichlorodehydroabietic acid (**4a**) was shown to activate the BK channel through interaction with the α subunit.[24c] It seems reasonable to assume that the hexahydrodibenzazepinone derivatives (**13**) also interact with the α subunits of the BK channels.

We thus designed several dimeric compounds, **27–29**, in which two units of the pharmacophore, dichlorohexahydrodibenzazepinone **13a**, are linked through the rigid diacetylenebenzene unit. Because we have little information about the arrangement and topology of the binding sites, we added adjustable molecular-dynamic flexibility by using an *n*-propyl chain as a tether between the nitrogen atom of the hexahydrodibenzazepinone core and the rigid diacetylenyl benzene core. Ortho, meta, and para substitution can change the direction of extension of

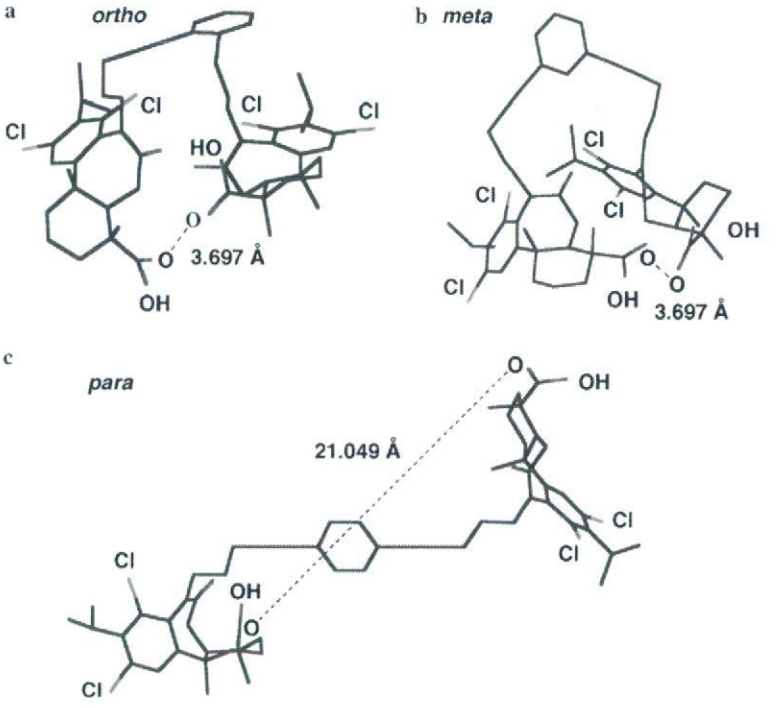

Figure 1. Conformational spaces of isomeric dimer compounds energy-minimized structures of the dimers in an *n*-octanol environment.

the two pharmacophores, and this molecular design allowed us to change the distance between the two pharmacophores in the dimer. In fact, molecular dynamic calculations on the basis of conformational search with OPLS2001 force field parameters in an *n*-octanol environment (Macromodel 8.5) generated a range of dimer structures.[27] We obtained various numbers of independent structures as follows: ortho (**27**): 2852 structures; meta (**28**): 2581 structures; para (**29**): 2838 structures, when the number of generated trial structures was set to 3000 in each case. The minimum-energy structures in each case are shown in Figure 1. The structural space was not significantly different in the gas-phase or in water as a solvent (data not shown). Because the carboxylic acid group of dehydroabietic acid **4** is known to be essential for BK channel opening activity,[24] this group presumably plays an important role in the interaction with the channel proteins. A similar role of the carboxylic acid group was expected for the hexahydrodibenzazepinone derivatives. The average (with standard deviation) minimum and maximum distances between the two carbonyl oxygen atoms of the individual carboxylic acids in the calculated dimer structures are as follows: ortho (**27**): 6.54 ± 4.02 Å (minimum: 3.01 Å; maximum: 15.37 Å); meta (**28**): 7.04 ± 5.54 Å (minimum: 2.99 Å; maximum: 18.42 Å); para (**29**): 22.23 ± 1.66 Å (minimum: 4.40 Å; maximum: 25.09 Å). The distances between the pharmacophores, particularly those of the carboxylic acids of **27**–**29**, accord well with the size of the pores of the K^+ channels, which are well conserved among the K^+ channel superfamily. The present designed dimeric compounds should be able to bind to the two putative binding sites of a single BK channel, if the binding sites are located close to the pore regions, and this should result in an increase of channel opening activity.

3. Results and discussion

3.1. Electrophysiological studies of hexahydrodibenzazepinones derivatives

The activity of the monomeric hexahydrodibenzazepinone derivatives as BK channel openers was evaluated by the patch–clamp technique with inside-out configuration. Human BK channel subunits, hSlo α and β_1, were transiently expressed in tsA201 cells, a derivative of the human embryonic kidney (HEK) cell line 293. In the patch–clamp measurement, when a compound has channel opening activity, the conductance–voltage curve shifts towards the negative voltage direction (leftward), that is, a larger BK channel current is activated by the same voltage step under the voltage–clamp condition. The BK channel opening activities of the tested compounds at 10 μM are represented as the shift of $V_{1/2}$ value (mV, $n = 3$–5), the voltage activating the half-maximum current, in comparison with the negative control in the presence of 100 μM Ca^{2+} on the intracellular side of the membrane patch (Fig. 2). In this work, we used dichlorodehydroabietic acid **4a** as a reference compound which has a related structure.[24]

The voltage shift of $V_{1/2}$ of **4a** was −5.3 ± 3.7 mV, and that of the *N*-methyl derivative of the hexahydrodibenzazepinone **13a** was −9.2 ± 3.7 mV. Compound **13a** can open the BK channel, while **13b**, its counterpart lacking the dichloro-substituent, did not show channel

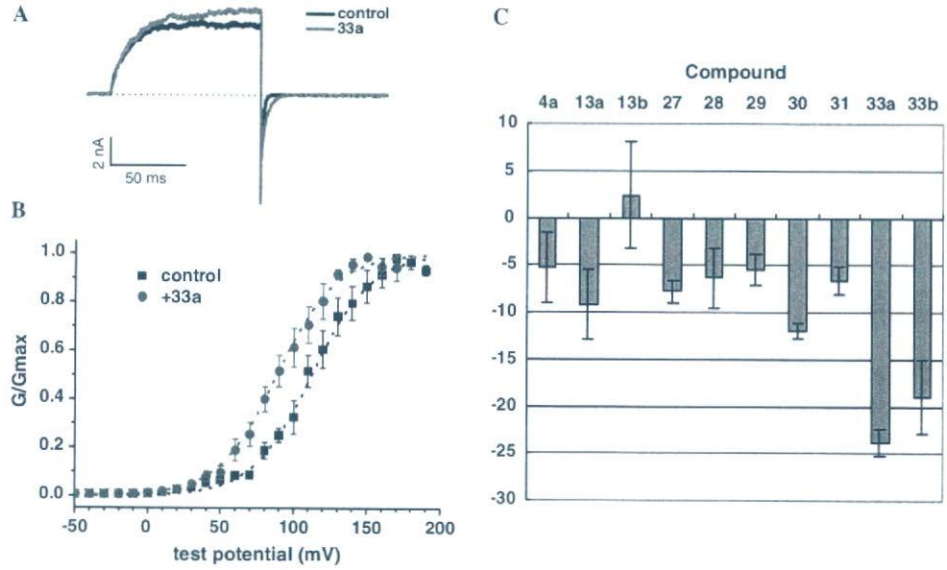

Figure 2. Effects of test compounds on the BK channel current. (A) Effect of **33a** on BK channel currents recorded in the inside-out macro patch-clamp configuration. BK channel currents were activated by test pulses to 100 mV from a holding potential at −100 mV. Current zero level is indicated by a dotted line. Outward BK channel currents are shown in upward direction. (B) Conductance–voltage relationship (G–V curve) of BK channel currents ($n = 4$). Compound **33a** shifted G–V curve toward hyperpolarized direction. (C) Shifts of $V_{1/2}$ value (mV) of G–V curve by test compounds ($n = 3$–5). A negative value indicates a shift to hyperpolarizing voltages.

opening activity. In this context, the results of the smooth muscle relaxation assay are consistent with those of the patch–clamp experiments.

Thus, the results of the electrophysiological study supported the idea that the dichloro-substituted *N*-methyl-hexahydrodibenzazepinone **13a** can serve as a pharmacophore for BK channel openers.

3.2. Electrophysiological study of the dimers and N-substituent effects

These dimeric compounds bearing dichloro substituents on the aromatic ring (**27**–**29**) were studied by means of an inside-out patch–clamp configuration. They showed BK channel opening activities, the left-shift of $V_{1/2}$ being -7.7 ± 1.2 mV, -6.3 ± 3.2 mV, and -5.4 ± 1.6 mV, respectively. While the channel opening activity of the ortho derivative **27** is likely to be stronger than those of the other isomers (**28** and **29**), the differences are not significant. In addition, the magnitude of the shift of **27** was as large as that of the monomer **13a**. These results imply that a part of the structures common to these dimeric isomers could be responsible for the activity, rather than the dual binding of the dimeric compounds to multiple binding sites of the BK channel. Thus, we synthesized monomeric fragments of the dimers, that is, **31** and **33a**, the former bearing a *N*-alkyl acetylene substituent and the latter bearing an additional terminal benzene moiety. We examined the BK channel opening activity of these compounds in patch clamp experiments (Fig. 2). Unexpectedly, we found that **33a** showed significant channel opening activity (-23.9 ± 1.4 mV left-shift of $V_{1/2}$), while **31** showed activity (-6.6 ± 1.5 mV) comparable in magnitude with that of the *N*-methyl derivative **13a**.

The prototype *N*-methyl hexahydrodibenzazepinone **13b**, lacking the aromatic dichloro-substituents, did not show BK channel opening activity in patch–clamp experiments (Fig. 2). However, the *m*-dimeric compound **30** showed channel opening activity with a hyperpolarizing shift of $V_{1/2}$ by -11.9 ± 0.9 mV. This activity is also probably derived from the fragment structure of the dimer. In fact, the monomeric compound **33b** also showed a strong opening activity, with a leftward shift of $V_{1/2}$ by -18.9 ± 3.8 mV, which is less than the shift caused by **33a**, but comparable in magnitude. The most potent compound **33a** expanded the width of the tail current in the patch-clamp measurements (data not shown), which suggests that this compound stabilizes the BK channel in the open state.

3.3. Isolated rabbit detrusor smooth muscle assay as overall activity

We evaluated the overall activities of hexahydrodibenzazepine derivatives on detrusor smooth muscle. Figure 3 shows the results of the rabbit detrusor smooth muscle assay. The K^+ channel-dependent muscle dilating effect was evaluated as follows.[28] Prior to the application of test compounds, detrusor smooth muscle strips were precontracted by depolarization caused by raising the extracellular K^+ concentration to either 30 mM or 120 mM. With the extracellular K^+ concentration at 30 mM, the small depolarization allows Ca^{2+} influx through Ca^{2+} channels to produce contraction. If a test compound activates the BK channel, the K^+ efflux will shift the membrane potential toward the equilibrium potential for K^+ (E_K) of approximately −40 mV where Ca^{2+} channels are closed, thus causing relaxation of the muscle strip. In contrast, with the extracellular K^+ concentration at 120 mM, the opening

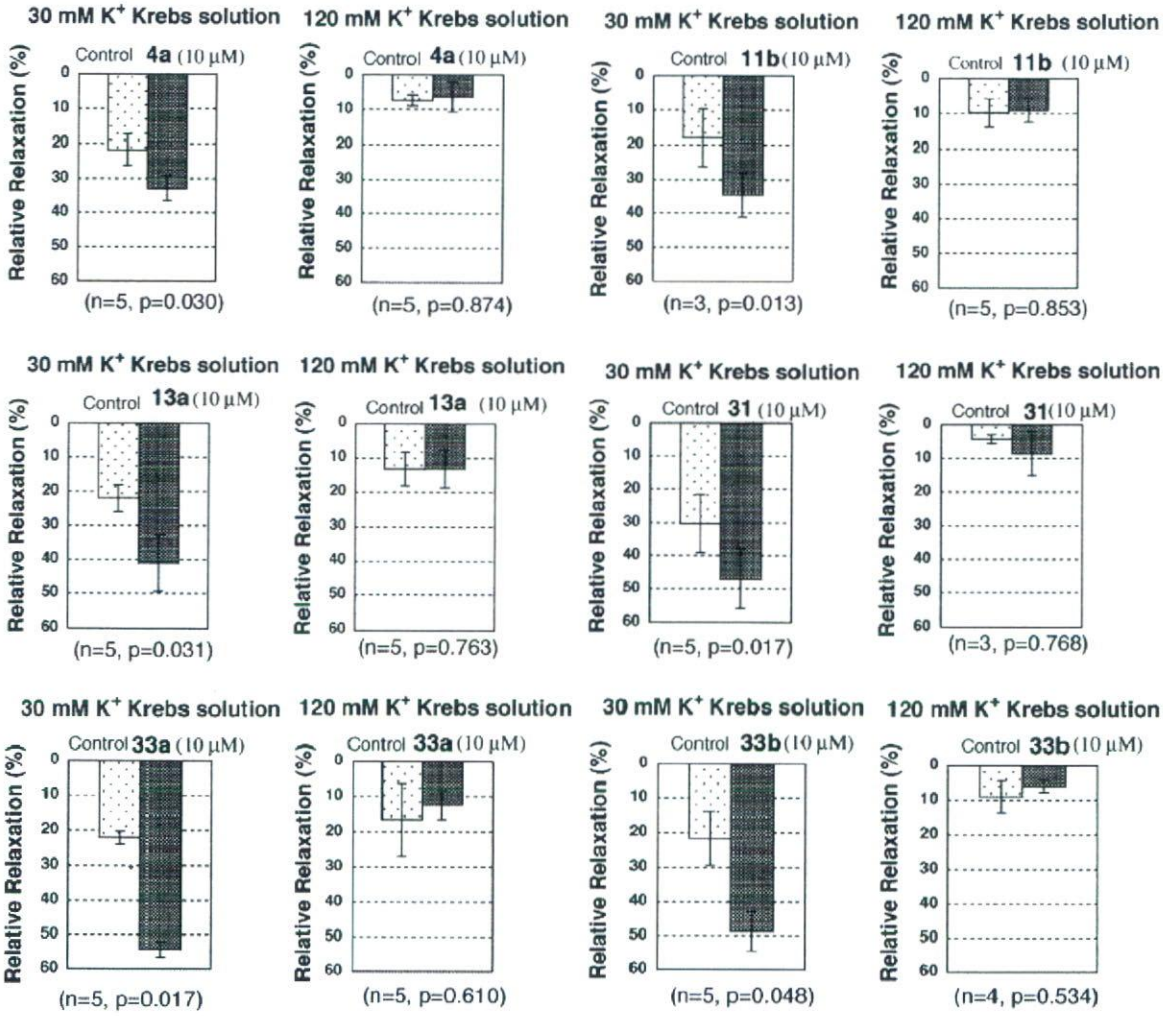

Figure 3. Detrusor smooth muscle relaxation assay The relative magnitude of relaxation was normalized to the precontraction caused by high K^+ (30 mM or 120 mM) as 100%. The relaxant activities of the test compounds were compared with that of 0.1% DMSO as the vehicle (control).

of the BK channel will shift the membrane potential toward E_K of around 0 mV, where Ca^{2+} channels are open, and the dilating activity of the BK channel opener should be abolished. The relative magnitude of relaxation was normalized to the contraction caused by high K^+ precontraction as 100%. The concentration of DMSO as a vehicle was set to be no more than 0.1% (v/v), because DMSO at high concentration caused relaxation by itself. Moreover, the concentration of the test compounds was fixed at 10 μM because of their relatively poor solubility in DMSO–water. The relaxant activities of the test compounds were compared with that of vehicle (0.1% DMSO) measured in the same muscle strip. All values are expressed as means ± SEM. Statistical significance of differences was determined by paired Student's *t*-test, and *P* values less than 0.05 were considered to be significant.

The results of the isolated rabbit detrusor smooth muscle relaxation study of the dehydroabietic acid derivatives were consistent with what we had found in the previous[24] and present electrophysiological studies. The dichloro-substituted **4a** showed a statistically significant relaxation activity, while the unsubstituted **4b** showed weak activity (data not shown). The smooth muscle relaxation study showed that the *N*-methyl derivative **13a**, bearing aromatic dichloro substituents, showed a statistically significant relaxation effect, while the prototype NH amide **11a** showed less potent activity (data not shown). Even in the absence of the aromatic dichloro substituents, the NH derivative **11b** showed distinct relaxation activity, while the *N*-methyl derivative **13b** did not.

The monomeric compounds **31** and **33a** showed distinct rabbit urinary bladder relaxation activities in detrusor smooth muscle strips (54.3 ± 2.3% and 48.68 ± 5.8%, respectively, $n = 5$), the activity of **33a** being statistically significant (Fig. 3). Reasonably, the N-alkylated monomeric compound **33b** also exhibited potent relaxation activities (48.68 ± 5.8%, $n = 5$).

4. Conclusion

In this work, we first demonstrated that the hexahydrodibenzazepinone structure represents a new scaffold for BK channel openers. Second, we carried out molecular design based on our hypothesis that dual binding of linked pharmacophores might provide strong activation even if the single pharmacophore is a rather weak opener. We found that the dimerization retained (in the case of **27**) or increased (in the case of **30**) the channel opening activity as compared with the corresponding monomeric pharmacophores (**13a** and **13b**, respectively). In the present design, ortho, meta, and para isomers (**27**–**29**) of the dimeric compounds showed similar, not increased, magnitudes of activity as compared with the minimal monomer **13a**, probably because the two pharmacophores cannot bind two putative binding sites at the same time. However, a portion of the molecules clearly can gain access to the binding site. Because of the highly hydrophobic nature of **33** and the dimers **27**–**30**, and retention of the opening activities of the dimers **27**–**30**, it is possible that there are hydrophobic binding sites in the transmembrane region of the channels which allow these hydrophobic molecules to gain access in a well-ordered conformation (at least partially) via a membrane bilayer pathway, rather than a direct aqueous pathway.[29] Finally, we found that the phenyl-bearing alkynyl substituent on the lactam amide nitrogen atom is crucial for BK channel opening activity. Our findings provide a new basis for development of novel BK channel openers.

5. Experimental

5.1. Chemistry

Commercially available reagents were purchased and were used without further purification unless otherwise stated. ^{1}H NMR spectra were recorded on a Bruker Advance (400 MHz) spectrometer. The chemical shifts (ppm) were shown by using tetramethylsilane (TMS) as an internal standard in deuterated chloroform ($CDCl_3$), and the peak of the solvent was used as an internal standard in the case of deuterated methanol (CD_3OD). Mass spectra were recorded on a JEOL MStation JMS-700 spectrometer. Elemental analyses were recorded on a Yanaco CHN CORDER spectrometer and were carried out at the Analysis Center of the Graduate School of Pharmaceutical Sciences, the University of Tokyo. Flash column chromatography was carried out with silica gel (Kanto Chemical 60 N, particle size 40–50 mm). Melting points were measured on a Yanaco hot-stage microscope and are uncorrected. Yields are shown in terms of those of isolated pure materials.

12,14-Dichlorodehydroabietic acid (4a). To a suspension of dehydroabietic acid **4b** (2.0 g, 6.66 mmol), 2% w/w $FeCl_3$ on SiO_2 (1 g), and 1% w/w DDQ on SiO_2 (0.1 g) in 25 mL CCl_4 was added a solution of 2.8 M Cl_2 in 35.7 mL CCl_4 (99.9 mmol, 15 equiv) at 0 °C. The reaction mixture was vigorously stirred at rt for one day in a sealed tube. Then to this mixture was added a solution of 2.8 M Cl_2 in 10 mL CCl_4 (28.0 mmol, 4 equiv) at rt, and the whole was stirred for 4 days. The insoluble materials were filtered off and the filtrate was then evaporated in vacuum. The residue was recrystallized from *n*-hexane to afford **4a** (574 mg, 1.554 mmol, yield 23%). Compound **4a**: colorless fine needles. Mp 218–222 °C (*n*-hexane/AcOEt). ^{1}H NMR ($CDCl_3$) 1.20 (3H, s, CH_3), 1.28 (3H, s, CH_3), 1.39 (6H, d, J = 7.3 Hz, 2CH_3CH), 1.61–1.66 (2H, m, 2CH), 1.72–1.86 (5H, m, 5CH), 2.13 (1H, dd, J = 12.6 Hz, 2.2 Hz, CH), 2.24 (1H, d, J = 11.9 Hz, CH), 2.70–2.79 (1H, m, CH), 2.94 (1H, dd, J = 18.4 Hz, 6.0 Hz, CH), 3.91 (1H, br s, CH_3C*H*), 7.15 (1H, s, ArH). MS (FAB$^+$) *m*/*z* 369 ([M(^{35}Cl$_2$)+H]$^+$), 371 ([M(^{35}Cl^{37}Cl)+H]$^+$), 373 ([M(^{37}Cl$_2$)+H]$^+$). Anal. Calcd for $C_{20}H_{26}Cl_2O_2$: C, 65.04; H, 7.10. Found: C, 64.95; H, 7.16.

12,14-Dichlorodehydroabietic acid methyl ester (6a). To a solution of 12,14-dichlorodehydroabietic acid **4a** (442 mg, 1.197 mmol) in MeOH (2 mL) and PhMe (4 mL) was dropwise added 2.0 M $TMSCHN_2$ in Et_2O (0.78 mL, 1.557 mmol, 1.3 equiv) at rt over 5 min, and the whole was stirred at rt for 30 min. Excess $TMSCHN_2$ was quenched with Et_2O, then the reaction mixture was evaporated in vacuum, and the residue was purified by flash chromatography (*n*-hexane only to *n*-hexane/AcOEt = 10:1) to afford **6a** (453 mg, 1.181 mol, yield 99%) as a colorless solid. **6a**: colorless needles. Mp 126–129 °C. ^{1}H NMR ($CDCl_3$) 1.19 (3H, s, CH_3), 1.26 (3H, s, CH_3), 1.39 (6H, d, J = 7.1 Hz, 2CH_3CH), 1.47–1.53 (2H, m, 2CH), 1.65–1.75 (5H, m, 5CH), 2.12 (1H, d, J = 10.6 Hz, CH), 2.23 (1H, d, J = 11.7 Hz, CH), 2.71–2.73 (1H, m, CH), 2.92 (1H, did, J = 18.3 Hz, 6.2 Hz, CH), 3.67 (3H, s, CO_2CH_3), 3.91 (1H, br s, CH_3C*H*), 7.15 (1H, s). LRMS (FAB$^+$) *m*/*z* 383 ([M(^{35}Cl$_2$)+H]$^+$), 385 ([M(^{35}Cl^{37}Cl)+H]$^+$), 387 ([M(^{35}Cl$_2$)+H]$^+$). Anal. Calcd for $C_{21}H_{28}Cl_2O_2$: C, 65.79; H, 7.36. Found; C, 65.86; H, 7.14.

Dehydroabietic acid methyl ester (6b). A mixture of dehydroabietic acid **4b** (5.1 g, 0.017 mol) and concd H_2SO_4 (6 mL) in MeOH (200 mL) was stirred at 85 °C for 19 h. Then concd H_2SO_4 (2 mL) was carefully added to the reaction mixture. Stirring was continued for 2 days, then the mixture was cooled, the solvent was evaporated in vacuum, and the residue was diluted with water (300 mL). The whole was extracted with $CHCl_3$ (1× 200 mL, 2× 100 mL). The combined organic layer was washed with brine (1× 100 mL), dried over Na_2SO_4, filtered, and then the solvent was evaporated in vacuum. The residue was purified by flash chromatography (*n*-hexane/AcOEt = 10:1) to afford **6b** (4.4 g, 0.014 mol, yield 83%) as a colorless solid. Compound **6b**: colorless needles. Mp 45–49 °C (*n*-hexane). ^{1}H NMR ($CDCl_3$) 1.21–1.23 (9H, m, 2CH_3CH and CH_3), 1.27 (3H, s, CH_3), 1.42 (1H, m, CH), 1.50 (1H, m, CH), 1.61–1.70 (5H, m, 5CH_2), 2.24 (1H, dd, J = 12.5 Hz, 2.1 Hz, CH), 2.30 (1H, d, J = 12.3 Hz, CH), 2.80–2.84 (1H, m, CH_3C*H*), 2.86–2.90 (1H, m, CH), 3.66 (3H, s, $COCH_3$), 6.88 (1H, s, ArH), 6.99 (1H, d, J = 6.4 Hz, ArH), 7.16 (1H, d, J = 8.1 Hz, ArH). LRMS (FAB$^+$) *m*/*z* 315

([M+H]$^+$). Anal. Calcd for $C_{21}H_{30}O_2$: C, 80.21; H, 9.62. Found: C, 80.07; H, 9.82.

13-Isopropyl-12,14-dichloro-7-oxopodocarpe-8,11,13-triene-15-carboxylic acid methyl ester (7a). To a solution of CrO_3 (287 mg, 2.867 mmol, 1.1 equiv) in Ac_2O (9 mL) and AcOH (4 mL) was dropwise added a suspension of the methyl ester **6a** (999 mg, 2.606 mmol) in AcOH (15 mL) at 0 °C over 10 min. The reaction mixture was stirred at 50 °C for 9 h, the whole was cooled, and poured into ice-water (40 mL) and then the whole was extracted with $CHCl_3$ (3× 30 mL). The combined organic layer was washed with water (1× 30 mL), satd $NaHCO_3$ (2× 30 mL), and brine (1× 30 mL), dried over Na_2SO_4, filtered, and then the solvent was evaporated in vacuum. The residue was purified by flash chromatography (*n*-hexane/AcOEt = 5:1) to afford **7a** (847 mg, 2.130 mmol, yield 82%) as a pale yellow amorphous solid. Compound **7c**: ^{1}H NMR ($CDCl_3$) 1.17 (3H, s, CH_3), 1.34 (3H, s, CH_3), 1.41 (6H, d, J = 7.3 Hz, 2CH_3CH), 1.75–1.79 (5H, m, 5CH), 2.20 (1H, d, J = 12.5 Hz, CH), 2.51 (1H, dd, J = 16.9 Hz, 5.2 Hz, CH), 2.64 (2H, m, 2CH), 3.66 (3H, s, CO_2CH_3), 3.94 (1H, br s, CH_3CH), 7.19 (1H, br s, ArH).

12,14-Dichloro-13-isopropyl-7-hydroxyiminepodocarpe-8,11,13-triene-15-carboxylic acid methyl ester (8a). A mixture of the methyl ester **7a** (198 mg, 0.498 mmol), pyridine (0.06 mL), and NH_2OH·HCl (54 mg, 0.772 mmol, 1.6 equiv) in EtOH (2 mL) was stirred at 100 °C for 3.5 h, the whole was cooled, and the solvent was evaporated in vacuum. The residue was purified by flash chromatography (*n*-hexane/AcOEt = 5:1) to afford **8a** (207 mg, quantitative yield) as a colorless amorphous solid. Compound **8a**: ^{1}H NMR ($CDCl_3$) 1.06 (3H, s, CH_3), 1.22 (6H, d, J = 8.4 Hz, 2CH_3CH), 1.26 (1H, dd, J = 18.7 Hz, 6.4 Hz, CH), 1.72–1.77 (5H, m, 5CH), 2.15 (2H, dd, J = 12.1 Hz, 6.1 Hz, CH), 2.38 (1H, dd, J = 18.7 Hz, 6.4 Hz, CH), 3.09 (1H, dd, J = 18.7 Hz, 13.0 Hz, CH), 3.66 (3H, s, CO_2CH_3), 3.69 (1H, br s, CH_3CH), 7.15 (1H, s, ArH).

12,14-Dichloro-13-isopropyl-7-tosyloxyiminepodocarpe-8,11,13-triene-15-carboxylic acid methyl ester (9a). To a solution of the methyl ester **8a** (207 mg, 0.503 mmol) in pyridine (1 mL) was added TsCl (144 mg, 0.754 mmol, 1.5 equiv) at rt. The reaction mixture was stirred for 17 h at rt, and then the solvent was evaporated in vacuum. The residue was purified by flash chromatography (*n*-hexane/AcOEt = 5:1) to afford **9a** (282 mg, 0.497 mmol, yield 99%) as a colorless oil. Compound **9a**: ^{1}H NMR ($CDCl_3$) 1.03 (3H, s, CH_3), 1.25 (3H, d, J = 7.1 Hz, CH_3CH), 1.27 (3H, d, J = 7.1 Hz, CH_3CH), 1.37 (3H, s, CH_3), 1.74–1.77 (5H, m, 5CH), 2.06–2.15 (2H, m, 2CH), 2.46 (3H, s, CH_3), 2.51 (1H, dd, J = 13.8 Hz, 5.0 Hz, CH), 3.02 (1H, dd, J = 19.0 Hz, 12.9 Hz, CH), 3.67 (3H, s, CO_2CH_3), 3.94 (1H, br s, CH_3CH), 7.12 (1H, br s, ArH), 7.35 (2H, d, J = 8.4 Hz, ArH), 7.94 (2H, d, J = 8.2 Hz, ArH).

12,14-Dichloro-13-isopropyl-8,11a-dimethyl-6-oxo-6,7,7a,8,9,10,11,11a-octahydro-5*H*-dibenzo[*b*,*d*]azepine-8-carboxylic acid methyl ester (10a). The mixture of the methyl ester **9a** (282 mg, 0.497 mmol) in TFA (2 mL) was stirred at rt for 1 h, and then the solvent was evaporated in vacuum. The residue was purified by flash chromatography (*n*-hexane/AcOEt = 1:1) to afford **10a** (166 mg, 0.403 mmol, yield 81%) as a colorless amorphous solid. Compound **10a**: ^{1}H NMR ($CDCl_3$): 1.42 (6H, d, J = 7.1 Hz, 2CH_3CH), 1.45 (3H, s, CH_3), 1.58 (3H, s, CH_3), 1.67–1.76 (2H, m, 2CH), 1.81–1.83 (2H, m, 2CH), 1.90–1.93 (2H, m, 2CH), 2.29 (1H, d, J = 8.6 Hz, CH), 2.92 (1H, dd, J = 15.9 Hz, 6.8 Hz, CH), 3.47–3.55 (1H, m, CH), 3.64 (3H, s, CO_2CH_3), 3.96 (1H, br s, CH_3CH), 7.26 (1H, br s, ArH), 7.85 (1H, br s, NH). LRMS (FAB$^+$) *m/z* 412 ([M($^{35}Cl_2$)+H]$^+$), 414 ([M($^{35}Cl^{37}Cl$)+H]$^+$), 416 ([M($^{37}Cl_2$)+H]$^+$).

12,14-Dichloro-13-isopropyl-8,11a-dimethyl-6-oxo-6,7,7a,8,9,10,11,11a-octahydro-5*H*-dibenzo[*b*,*d*]azepine-8-carboxylic acid (11a). A mixture of the methyl ester **10a** (80 mg, 0.194 mmol), KOH (109 mg, 3.068 mmol, 10.0 equiv), and 18-crown ether-6 (128 mg, 0.485 mmol, 2.5 equiv) in MeOH (2 mL) was stirred at 80 °C for 7.5 h, the whole was cooled, and then the solvent was evaporated in vacuum. The residue was diluted with water (10 mL), acidified with 2 N HCl (2 mL), and the whole was extracted with $CHCl_3$ (3× 20 mL). The combined organic layer was washed with brine (1× 20 mL), dried over Na_2SO_4, filtered, and then the solvent was evaporated in vacuum. The residue was purified by flash chromatography (AcOEt only to AcOEt/MeOH = 10:1) to afford **11a** (35 mg, 0.087 mmol, yield 45%) as a colorless solid. Compound **11a**: colorless powder. Mp 192–197 °C (*n*-hexane/AcOEt/MeOH). ^{1}H NMR (CD_3OD): 1.32 (6H, d, J = 7.1 Hz, 2CH_3CH), 1.36 (3H, s, CH_3), 1.47 (3H, s, CH_3), 1.60 (2H, m, 2CH), 1.70 (2H, m, 2CH), 1.70 (2H, m, 2CH), 1.85 (2H, m, 2CH), 2.10 (1H, d, J = 8.4 Hz, CH), 2.86 (1H, dd, J = 15.9 Hz, CH), 3.27 (1H, m, CH), 3.90 (1H, br s, CH_3CH), 7.23 (1H, br s, ArH). LRMS (FAB$^+$) *m/z* 398 ([M($^{35}Cl_2$)+H]$^+$), 400 ([M($^{35}Cl^{37}Cl$)+H]$^+$), 402 ([M($^{37}Cl_2$)+H]$^+$). Anal. Calcd for $C_{20}H_{25}Cl_2NO_3$·3/4H_2O: C, 58.33; H, 6.30; N, 3.40. Found: C, 58.29; H, 6.39; N, 3.39.

13-Isopropyl-7-oxopodocarpe-8,11,13-triene-15-carboxylic acid methyl ester (7b). To a solution of CrO_3 (790 mg, 7.886 mmol, 1.1 equiv) in Ac_2O (28 mL) and AcOH (14 mL) was dropwise added a suspension of dehydroabietic acid methyl ester **6b** (2.35 g, 7.456 mmol) in AcOH (6 mL) at rt for 11 min. The reaction mixture was stirred for 15 min at rt, then stirred at 50 °C for 8.5 h. The mixture was cooled, and the whole was poured into icewater (100 mL) and then extracted with $CHCl_3$ (1× 200 mL, 2× 100 mL). The combined organic layer was washed with brine (1× 100 mL), dried over Na_2SO_4, filtered, and then the solvent was evaporated in vacuum. The residue was purified by flash chromatography (*n*-hexane/AcOEt = 5:1) to afford the desired compound **7b** (570 mg, 1.746 mmol, yield 23%) as a pale yellow oil and the undesired overreacted compound (550 mg, 1.431 mmol, yield 19%) as a yellow oil. Compound **7b**: ^{1}H NMR ($CDCl_3$) 1.24–1.26 (9H, m, 2CH_3CH and CH_3), 1.34 (3H, s, CH_3), 1.61–1.80 (5H, m, 5CH), 2.32–2.38 (2H, m, 2CH), 2.71–2.73 (2H, m, 2CH), 2.91–2.95 (1H, m, CH_3CH), 3.65 (3H, s, CO_2CH_3), 7.29 (1H, d, J = 8.1 Hz, ArH), 7.40 (1H, dd, J = 8.2 Hz, 2.1 Hz, ArH), 7.87 (1H, d, J = 2.0 Hz,

ArH). LRMS (FAB$^+$) *m/z* 329 ([M+H]$^+$). *By-product:* (13-(1-Acetoxy-1-methylethyl)-7-oxopodocarpe-8,11,13-triene-15-carboxylic acid methyl ester): ^{1}H NMR ($CDCl_3$) 1.26 (3H, s, CH_3), 1.34 (3H, s, CH_3), 1.72–1.79 (1H, m, 5CH and 2CH_3CPh), 2.10 (3H, s, CH_3CO), 2.32–2.36 (2H, m, 2CH), 2.70–2.74 (2H, m, 2× CH), 3.66 (3H, s, CO_2CH_3), 7.33 (1H, d, J = 8.2 Hz, ArH), 7.52 (1H, dd, J = 8.3 Hz, 2.3 Hz, ArH), 7.97 (1H, d, J = 2.4 Hz, ArH).

13-Isopropyl-7-hydroxyiminepodocarpe-8,11,13-triene-15-carboxylic acid methyl ester (8b). A mixture of the methyl ester **7b** (598 mg, 1.667 mmol), pyridine (0.2 mL), and NH_2OH·HCl (180 mg, 2.585 mmol, 1.6 equiv) in EtOH (4 mL) was stirred at 100 °C for 3 h, the mixture was cooled, and the solvent was evaporated in vacuum. The residue was purified by flash chromatography (*n*-hexane/AcOEt = 5:1) to afford **8b** (390 mg, 1.137 mmol, yield 68%) as a colorless amorphous solid. Compound **8b**: ^{1}H NMR ($CDCl_3$) 1.12 (3H, s, CH_3), 1.25 (6H, d, J = 7.0 Hz, 2CH_3CH), 1.38 (3H, s, CH_3), 1.42–1.76 (5H, m, 5CH), 2.28–2.35 (2H, m, 2CH), 2.64–2.67 (2H, m, 2CH), 2.88–2.91 (1H, m, CH_3CH), 3.65 (3H, s, CO_2CH_3), 7.21 (2H, m, ArH), 7.70 (1H, s, ArH). LRMS (FAB$^+$) *m/z* 344 ([M+H]$^+$).

13-Isopropyl-7-tosyloxyiminepodocarpe-8,11,13-triene-15-carboxylic acid methyl ester (9b). To a solution of the methyl ester **8b** (390 mg, 1.137 mmol) in pyridine (1 mL) was added TsCl (325 mg, 1.705 mmol, 1.5 equiv) at rt. The reaction mixture was stirred for 14 h at rt, and then the solvent was evaporated in vacuum. The residue was purified by flash chromatography (*n*-hexane/AcOEt = 5:1) to afford **9b** (545 mg, 1.095 mmol, yield 96%) as a colorless solid. Compound **9b**: colorless powder. Mp 158–160 °C (*n*-hexane/AcOEt). ^{1}H NMR ($CDCl_3$) 1.04 (3H, s, CH_3), 1.20–1.28 (6H, m, 2CH_3CH), 1.34 (3H, s, CH_3), 1.68–1.74 (5H, m, 5CH), 2.26 (2H, t, J = 9.3 Hz, CH_2), 2.45 (3H, s, PhCH_3), 2.66 (2H, d, J = 8.6 Hz, CH_2), 2.85–2.88 (1H, m, CH_3CH), 3.66 (3H, s, CO_2CH_3), 7.18 (1H, d, J = 8.2 Hz, ArH), 7.25 (1H, dd, J = 8.2 Hz, 2.0 Hz, ArH), 7.35 (2H, d, J = 8.6 Hz, ArH), 7.58 (1H, d, J = 1.8 Hz, ArH), 7.95 (2H, d, J = 8.4 Hz, ArH). LRMS (FAB$^+$): *m/z* 498 ([M+H]$^+$). Anal. Calcd for $C_{28}H_{35}NO_5S$: C, 67.58; H, 7.09; N, 2.81. Found: C, 69.39; H, 7.21; N, 2.91.

13-Isopropyl-8,11a-dimethyl-6-oxo-6,7,7a,8,9,10,11,11a-octahydro-5*H*-dibenzo[*b*,*d*]azepine-8-carboxylic acid methyl ester (10b). A mixture of the methyl ester **9b** (505 mg, 1.015 mmol) in TFA (3 mL) was stirred at rt for 40 min, and then the solvent was evaporated in vacuum. The residue was purified by flash chromatography (*n*-hexane/AcOEt = 1:1) to afford **10b** (392 mg, quantitative yield) as a colorless amorphous solid. Compound **10b**: colorless needles. Mp 148–149 °C (*n*-hexane/AcOEt). ^{1}H NMR ($CDCl_3$) 1.24 (6H, d, J = 7.0 Hz, 2CH_3CH), 1.42 (3H, s, CH_3), 1.45 (3H, s, CH_3), 1.69–1.93 (6H, m, 6CH), 2.18 (1H, d, J = 14.8 Hz, CH), 2.57 (1H, dd, J = 14.7 Hz, 8.2 Hz, CH), 2.78–2.81 (1H, dd, J = 8.2 Hz, 3.6 Hz, CH), 2.85–2.88 (1H, m, CH_3CH), 3.65 (3H, s, CO_2CH_3), 6.76 (1H, d, J = 2.0 Hz, ArH), 7.04 (1H, d, J = 8.2 Hz, ArH), 7.33 (1H, d, J = 8.4 Hz, ArH), 8.62 (1H, s, NH). LRMS (FAB$^+$) *m/z* 343 ([M+H]$^+$). Anal. Calcd for $C_{21}H_{29}NO_3$: C, 73.44; H, 8.51; N, 4.08. Found: C, 73.21; H, 8.29; N, 4.10.

13-Isopropyl-8,11a-dimethyl-6-oxo-6,7,7a,8,9,10,11,11a-octahydro-5*H*-dibenzo[*b*,*d*] azepine-8-carboxylic acid (11b). A mixture of the methyl ester **10b** (100 mg, 0.291 mmol), KOH (163 mg, 2.911 mmol, 10.0 equiv) and 18-crown ether-6 (192 mg, 0.728 mmol, 2.5 eq.) in MeOH (2 mL) was stirred at 80 °C for 15 h, the whole was cooled, and the solvent was evaporated in vacuum. The residue was diluted with water (10 mL), acidified with 2 N HCl (2 mL), and then the mixture was extracted with $CHCl_3$ (3× 20 mL). The combined organic layer was washed with brine (1× 20 mL), dried over Na_2SO_4, filtered, and then the solvent was evaporated in vacuum. The residue was purified by flash chromatography (*n*-hexane/AcOEt = 1:2) to afford **11b** (75 mg, 0.228 mmol, yield 78%) as a colorless oil. Compound **11b**: colorless powder (*n*-hexane/AcOEt); Mp 135–140 °C; ^{1}H NMR ($CDCl_3$) 1.22 (6H, d, J = 6.8 Hz, 2CH_3CH), 1.42 (3H, s, CH_3), 1.45 (3H, s, CH_3), 1.74–1.88 (5H, m, 5CH), 1.95 (1H, d, J = 11.3 Hz, CH), 2.28 (1H, dd, J = 14.9 Hz, 3.4 Hz, CH), 2.67 (1H, dd, J = 14.9 Hz, 7.8 Hz, CH), 2.80 (1H, dd, J = 7.9 Hz, 3.7 Hz, CH), 2.83–2.86 (1H, m, CH_3CH), 6.70 (1H, d, J = 1.8 Hz, ArH), 7.00 (1H, dd, J = 8.0 Hz, 1.8 Hz, ArH), 7.31 (1H, d, J = 8.4 Hz, ArH), 7.99 (1H, s, ArH). LRMS (FAB$^+$) *m/z* 330 ([M+H]$^+$). Anal. Calcd for $C_{20}H_{27}NO_3$·1/6H_2O: C, 72.26; H, 8.28; N, 4.21. Found: C, 72.21; H, 8.15; N, 4.16.

12,14-Dichloro-3-isopropyl-5,8,11a-trimethyl-6-oxo-6,7,7a,8,9,10,11,11a-octahydro-5*H*-dibenzo[*b*,*d*]azepine-8-carboxylic acid methyl ester (12a). To a suspension of NaH (60% in mineral oil, washed twice with *n*-hexane) (10 mg, 0.244 mmol, 1.1 equiv) in DMF (1 mL) was dropwise added a solution of the methyl ester **10a** (91 mg, 0.222 mmol) in DMF (1 mL) at 0 °C for 2 min in a flask fitted with a $CaCl_2$ tube. After stirring at 0 °C for 15 min, MeI (0.07 mL, 1.108 mmol, 5.0 equiv) was added to the reaction mixture at 0 °C. Stirring was continued at rt for 7 h, the solvent was evaporated in vacuum, and the residue was diluted with 1NHCl (10 mL) and then extracted with $CHCl_3$ (3× 20 mL). The combined organic layer was washed with brine (1× 20 mL), dried over Na_2SO_4, filtered, and then the solvent was evaporated in vacuum. The residue was purified by flash chromatography (*n*-hexane/AcOEt = 2:1) to afford **12a** (73 mg, 0.171 mmol, yield 77%) as a colorless oil. Compound **12a**: ^{1}H NMR ($CDCl_3$) 1.36 (3H, s, CH_3), 1.42 (6H, d, J = 7.1 Hz, 2CH_3CH), 1.46 (3H, s, CH_3), 1.72–1.73 (2H, m, CH_2), 1.82–1.91 (4H, m, 4CH), 2.21 (1H, d, J = 8.6 Hz, CH), 2.74 (1H, d, J = 16.3 Hz, CH), 3.19 (3H, s, NCH_3), 3.64 (3H, s, CO_2CH_3), 3.81 (1H, dd, J = 16.2 Hz, 8.8 Hz, CH), 4.09 (1H, br s, CH_3CH), 7.20 (1H, br s, ArH).

12,14-Dichloro-13-isopropyl-5,8,11a-trimethyl-6-oxo-6,7,7a,8,9,10,11,11a-octahydro-5*H*-dibenzo[*b*,*d*]-azepine-8-carboxylic acid (13a). A mixture of the methyl ester **12a** (73 mg, 0.171 mmol), KOH (96 mg, 1.705 mmol, 10.0 equiv) and 18-crown ether-6 (113 mg, 0.426 mmol, 2.5 equiv) in MeOH (1 mL) was stirred at 80 °C for 13 h, the whole was cooled, and the solvent was evaporat-